European Journal of Pharmaceutical Sciences 193 (2024) 106673

Contents lists available at ScienceDirect

European Journal of Pharmaceutical Sciences

journal homepage: www.elsevier.com/locate/ejps

Cyclosporine A micellar nasal spray characterization and antiviral action against SARS-CoV-2

Fabiola Guareschi [a], Elena Del Favero [b], Caterina Ricci [b], Laura Cantù [b], Martina Brandolini [c], Vittorio Sambri [c,d], Sara Nicoli [a], Silvia Pescina [a], Davide D'Angelo [a], Irene Rossi [e], Francesca Buttini [a,f], Ruggero Bettini [a,f], Fabio Sonvico [a,f,*]

[a] ADDRes Lab, Department of Food and Drug, University of Parma, Parco Area delle Scienze 27/a, 43124 Parma, Italy
[b] Department of Medical Biotechnology and Translational Medicine, University of Milan, Via Fratelli Cervi 93, 20054 Milan, Italy
[c] Unit of Microbiology, The Great Romagna Hub Laboratory, Piazza della Liberazione 60, 47522 Pievesestina, Italy
[d] Department of Experimental, Diagnostic and Specialty Medicine—DIMES, Alma Mater Studiorum—University of Bologna, Via Massarenti 1, 40138 Bologna, Italy
[e] Nanopharm Ltd, Franklin House, Grange Road, Cwmbran NP44 3WY, United Kingdom
[f] Interdepartmental Center for Innovation in Health Products, Biopharmanet_TEC, University of Parma, Parco Area delle Scienze 27/A, 43124 Parma, Italy

ARTICLE INFO

Keywords:
Cyclosporine A
TPGS micelles
Nasal delivery
SARS-CoV-2
Antiviral activity
Nasal spray devices

ABSTRACT

The upper airways represent the point of entrance from where Severe Acute Respiratory Syndrome Coronavirus 2 (SARS-CoV-2) infection spreads to the lungs. In the present work, α-tocopheryl-polyethylene-glycol succinate (TPGS) micelles loaded with cyclosporine A (CSA) were developed for nasal administration to prevent or treat the viral infection in the very first phases. The behavior of the micelles in presence of simulated nasal mucus was investigated in terms of stability and mucopenetration rate, evidencing long-term stability and fast diffusion across the glycoproteins matrix. Moreover, the spray characteristics of the micellar formulation and deposition profile in a silicon nasal model were studied using three nasal spray devices. Results allowed to identify the nasal spray pump (BiVax, Aptar) able to provide the wider and uniform deposition of the nasal cavity. The cyclosporine A micelles antiviral activity against SARS-CoV-2 was tested on the Omicron BA.1 variant using Vero E6 cells with protocols simulating treatment before, during and after the infection of the upper airways. Complete viral inactivation was observed for the cyclosporine-loaded micelles while a very low activity was evidenced for the non-formulated drug, suggesting a synergistic activity of the drug and the formulation. In conclusion, this work showed that the developed cyclosporine A-loaded micellar formulations have the potential to be clinically effective against a wide spectrum of coronavirus variants.

1. Introduction

Severe acute respiratory syndrome coronavirus 2 (SARS-CoV-2) belongs to the coronavirus genus, which comprehends 26 (Liu et al., 2020) known species divided in four genera (Alpha, Beta, Gamma and Delta CoV) (Gorbalenya et al., 2020). However, only Alpha and Beta Coronaviruses can infect humans, leading to mild to severe respiratory infections (Gorbalenya et al., 2020). SARS-CoV-2 is a Betacoronavirus, discovered for the first time in Wuhan, China, at the end of 2019 and it since spread dramatically rapidly all over the world (Hu et al., 2021; Wu et al., 2020). This led to a pandemic which caused a significatively higher number of infected people and larger diffusion than the previously Severe Acute Respiratory Syndrome (SARS-CoV) and Middle East Respiratory Syndrome (MERS-CoV) coronaviruses appeared in 2002 and 2012, respectively (Hu et al., 2021). The infection can cause the manifestation of various symptoms comprehending fever and cough, but in the most severe cases, the rapid viral replication can lead to a strong immune response, consisting in a high release of cytokines. This cytokine "storm" can rapidly lead the patient to death, since it provokes acute respiratory distress syndrome and respiratory failure (Laforge et al., 2020; Mehta et al., 2020). Despite SARS-CoV-2 can infect all the human population regardless of the age and gender, older men with coexisting illnesses appears to be the fraction most exposed to the risk of developing a severe respiratory disease requiring hospitalization and often causing death (Chen et al., 2020).

Due to its unique virological features, SARS-CoV-2 shows a high

* Corresponding author.
E-mail address: fabio.sonvico@unipr.it (F. Sonvico).

https://doi.org/10.1016/j.ejps.2023.106673
Received 17 November 2023; Received in revised form 11 December 2023; Accepted 13 December 2023
Available online 14 December 2023

transmissibility. In particular, the transmission often occurs early since registered viral load in the upper airways has been found to be already very high when the first symptoms occur; this correlates with an high risk of nasopharyngeal virus shedding at the beginning of the infection (Lirong Zou et al., 2020; Wölfel et al., 2020). The airborne transmission of the virus from an infected person occurs through liquid droplets incorporating the virus during speech. Furthermore, together with the larger droplets, smaller and more numerous aerosol particles are produced. These latter can persist in the air for a long period of time and finally inhaled by someone thus leading to a starting infection (Bleier et al., 2020; Stadnytskyi et al., 2020). Therefore, after the starting infection of the epithelial cells located in the upper respiratory tract, the virus quickly migrates to the deeper airways and finally reaches the alveolar epithelial tissue in the lungs (Hu et al., 2021).

Vaccination is certainly one of the most effective tools to control and prevent the spread of viral pandemics (Chavda et al., 2023, 2021), but the genetic variability of the coronaviruses complicates the development of effective vaccination able to prevent the infection of all the viral variants (Liu et al., 2020). For this reason, a broad spectrum of drugs is currently being studied for their anti-viral properties against coronaviruses. Cyclosporine A belongs to this group, since already in 2011 it was demonstrated to be effective at suppressing coronaviruses on a broad spectrum (de Wilde et al., 2011). One peculiar viral replication feature of SARS-CoV-2 is that the virus exploits the activity of the intracellular cyclophilin A (CypA) when infecting the host cell. This highly-expressed protein provides the cloaking of the viral replication intermediates, thus preventing the viral nucleic acid to be detected by the innate immune cellular sensors (Mamatis et al., 2022). The mechanism of action of cyclosporine A consists precisely in the inhibition of CypA, (de Wilde et al., 2011; Liu et al., 2020) therefore hindering the viral cloaking step and leading to a restoration of the normal innate immunity processes including the expression of antiviral genes that block the viral infection (Mamatis et al., 2022). In addition to this, CSA can also be exploited to limit the excessive release of pro-inflammatory cytokines in patients infected with SARS-CoV-2 by creating a complex with CypA and calcineurin (CaN). In this complex, the phosphorylation activity of CaN, normally involved in the release of several pro-inflammatory cytokines, is inhibited (Peel and Scribner, 2013; Schreiber and Crabtree, 1992; Sweeney et al., 2014). Results from cell culture experiments have demonstrated that CSA strongly inhibits the replication of SARS-CoV, manifesting the antiviral activity only at the early stage of viral replication and at a relatively higher concentration (16 μM) if compared to that required to inhibit the replication of other RNA viruses (0.5 – 3 μM) (de Wilde et al., 2011; Pfefferle et al., 2011).

However, the peptide nature, the relatively high molecular weight (1202.635 Da), the low aqueous solubility (~ 5 μg/mL in phosphate buffered saline) (Berton et al., 2019; Lallemand et al., 2005) and the high lipophilicity attested by a log P value of 3, (El Tayar et al., 1993) make the formulation of CSA challenging.

One strategy to formulate CSA proposed in the past is represented by oil-based surfactant-containing dosage forms (Lallemand et al., 2017). However, these formulations when applied on mucosal tissues, such as the eye for instance, evidenced low tolerability causing local inflammatory responses, as irritation and hyperemia (Lallemand et al., 2003; Patel et al., 2013). Furthermore, it is suggested that because of the high affinity of the drug for the oily phase of pharmaceutical emulsions, in most cases these formulations show poor bioavailability (Patel et al., 2013). A possible valid alternative to emulsions is represented by micelles, able to increase the solubility of this hydrophobic peptide drug. Micelles are nanosystems relatively easy to prepare and characterized by high scalability which demonstrated to be able to improve the drug solubility and cellular uptake (Ghezzi et al., 2022; Pepić et al., 2013). Despite ocular administration of CSA, also in micellar formulations, has been extensively studied, (Ghezzi et al., 2022; Guo et al., 2005; Luschmann et al., 2014; Yu et al., 2018) to the best of our knowledge, CSA-loaded micelles have not yet been tested for intranasal administration as antiviral agents against SARS-CoV-2. However, it is reported in literature that a nasal spray containing nitric oxide has been used to efficiently reduce the SARS-CoV-2 viral RNA concentration in patients infected with the virus, confirming the efficacy of the intranasal approach to allow the clearance of the virus (Sonvico et al., 2023; Tandon et al., 2022).

Therefore, the aim of this study was to formulate and characterize cyclosporine A loaded micelles produced using a vitamin E derivative, *i.e.* α-tocopherol polyethylene glycol 1000 succinate (TPGS) and to evaluate their antiviral activity *in vitro* against SARS-CoV-2, in view of a clinical application via intranasal administration.

2. Materials and methods

2.1. Materials

The vitamin E-derived surfactant α-tocopherol polyethyleneglycol succinate (TPGS, MW 1513 g/mol) was a kind gift from PMC ISOCHEM (Vert-Le-Petit, France). Cyclosporine A (CSA, MW 1202.61 g/mol) was obtained from Metapharmaceutical (Barcelona, Spain). Deuterium oxide (D_2O) and mucin from porcine stomach type II were from Sigma Aldrich (Saint Louis, USA). Sodium chloride (NaCl) was obtained from VWR International (Leuven, Belgium). Calcium chloride ($CaCl_2$) was purchased from Fluka Chemika (Buchs, Switzerland). Potassium chloride (KCl) was provided by A.C.E.F (Fiorenzuola d'Arda, Italy). Acetonitrile, trifluoroacetic acid and the other solvents were of HPLC grade. Ultrapure water was purified by reverse osmosis (MilliQ, Millipore, Molsheim, France).

2.2. Methods

2.2.1. Preparation of the blank and drug-loaded micelles

The micelles were prepared following the method described previously by Pescina *et al.* (Pescina et al., 2021). For the preparation of the blank micelles, TPGS (20 mM, 3% w/v) was solubilized in a NaCl solution (9 g/L). The system was kept under magnetic stirring at 300 rpm until the complete dissolution of the TPGS. Importantly, the solution was prepared in a closed amber glass vessel to preserve TPGS from possible photodegradation.

The drug-loaded micelles were prepared by adding to the previously prepared blank micelles the CSA powder, accurately weighed on an aluminum weighing boat. More precisely, different amounts of CSA (1 mg, 2.5 mg and 5 mg) were used to prepare 10 mL of the Low-Loading (LL, 0.1 mg/mL), Medium-Loading (ML, 0.25 mg/mL) and High-Loading (HL, 0.5 mg/mL) micelles.

Then, the system was subjected to sonication in an ultrasound bath (USC 300-T, VWR International, Radnor, PA, USA) for 2 minutes to favor the complete detachment of the powder from the weighing boat. Finally, the micelles were maintained under magnetic stirring at 300 rpm (AREX-6 Digital, VELP Scientific, Usmate, Italy) overnight. To separate the eventual non-encapsulated drug, as a precipitate, the micelles were subjected to centrifugation (NEYA-16R, Remi Elektrotechnik, Vasai, India) at 9,500 rpm for 10 minutes at 25°C. The supernatant was finally collected and stored at 25°C in amber glass vessels.

2.2.2. Characterization and stability study

2.2.2.1. Particle size, PDI and surface Zeta Potential. The particle size and the polydispersity index (PDI) of both the blank and drug-loaded micelles were determined by dynamic light scattering (DLS) using Malvern Zetasizer Nano ZS (range 0.3 nm - 10 μm, Malvern Instruments Ltd., Malvern, UK). For each DLS measurement, 1 mL of the formulation was analyzed without dilution using a disposable polystyrene cuvette. Measurements were performed at the temperature of 25°C and at a scattering angle of 173°. The refractive index and the viscosity of the

dispersant were 1.33 and 0.8872 mPa·s, respectively. The refractive index of the material was set at the value of 1.00. Before analysis, the sample was equilibrated for 30 seconds. Analyses were repeated three times for each sample, with 15 sub-runs for measurement to increase data and correlation and reported as cumulative unimodal/multimodal fitting (sample dependent) and Z-average mean particles size.

The samples were also analyzed for zeta-potential using a patented laser interferometric technique called M3-PALS (Phase analysis Light Scattering), with the same instrument (Zetasizer Nano ZS, Malvern Instruments Ltd., Malvern, UK) and the same parameter set for particle size and PDI analysis. Analyses were performed using a disposable folded capillary cell, at 25°C, and recorded three times for each sample, with 100 runs for measurement.

The characterization of the produced micelles was done at time zero and after every month for 7 months, keeping the samples stored at 25°C in closed amber glass vessels.

DLS was also employed to evaluate any changes in terms of size before and after actuation of the micellar formulation from the nasal devices tested. To do this, the formulation was sprayed into 2 mL Eppendorf® tubes (Eppendorf AG, Hamburg, Germany) after being loaded into each nasal device tested. Then, the sample was collected and analyzed by DLS as described above.

2.2.2.2. Density. The densities of TPGS micellar formulations were assessed at 22°C with a density meter (DMA5000, Anton Paar, Graz, Austria) allowing an accuracy of 7×10^{-6} g/cm^3. Samples (1.5 mL) were inserted into the measuring U-capillary cell by means of two syringes, tightly connected at its ends, and were equilibrated for 15 minutes at each temperature before data collection.

2.2.2.3. Viscosity. Dynamic viscosity, η, was measured for the blank, HL, ML and LL micelles by a controlled shear rate MCR102 Rheometer and data were analyzed using the Rheocompass™ software version 1.25 (Anton Paar, Graz, Austria). Rotational measurements were carried out without diluting the samples, which were analyzed by a CC27 geometry (27 mm diameter, 1.13 mm gap). Measurements were performed both at 25°C and at 37°C to simulate the physiological nostril temperature, for a shear rate ranging from 10 to 1000 s^{-1}. All the analysis were performed in triplicate.

2.2.2.4. pH. The pH of the blank and the drug loaded micelles was determined by a SevenCompact™ pH meter S210 (Mettler Toledo, Milano, Italy). The measurements were performed in triplicate keeping the samples at room temperature.

2.2.2.5. Cyclosporine A quantification method. The method used to quantify the amount of solubilized drug in the drug-loaded micelles was previously validated for precision and accuracy (Grimaudo et al., 2018). Briefly, CSA was quantified using a HPLC-UV system consisted of a pump (Model LC-10 AS, Shimadzu, Japan) and an ultraviolet detector (Model SPD-10A, Shimadzu, Japan). The mobile phase was a mixture acetonitrile: water with 0.1% trifluoroacetic acid in 65:35 (v/v) ratio, pumped at 1.6 mL/min. The column used to analyze cyclosporine A was a reverse-phase Nova-Pack C18 cartridge (150 × 3.9 mm, 4 μm, Waters, Milford, MA, USA) equipped with a guard column (4 × 3.0 mm, Security Guard™ Cartridge, Phenomenex, USA) thermostated at 65°C. The injection volume was 100 μL and absorbance was monitored at 230 nm. Using these conditions, cyclosporine A retention time was about 4 minutes. The CSA stock solution was prepared by dissolving a weighed amount of CSA in acetonitrile. The dilutions of the stock were then prepared in mobile phase.

Several calibration curves were built to cover different concentration ranges: 3 – 90 μg/mL, used for the quantification of the drug loaded into the micelles; and 0.1 – 3 μg/mL and 1 – 10 μg/mL, exploited for the *ex vivo* mucoadhesion study. Each stock dilution of these two latter calibration curves was then diluted with water to generate two additional calibration curves in the ranges of 0.77 - 7.69 μg/mL and 0.08 – 2.3 μg/mL. These curves were used for the CSA quantification in samples deriving from the mucoadhesion experiments, which were diluted in an aqueous medium.

To extract the drug from the micelles, 100 μL of each micellar formulation was mixed with 900 μL of mobile phase; the sample were mixed and analyzed by HPLC.

The quantification of the solubilized drug was done at time 0 and after every month for 7 months, keeping the samples stored at 25°C in closed amber glass vessels.

2.2.2.6. SAXS and SANS analysis. Small Angle X-ray (SAXS) and Neutron (SANS) scattering measurements were carried at the high brilliance beamline ID02 of the European Synchrotron Radiation Facility (ESRF, Grenoble, France), experiment DOI: 10.15151/ESRF-ES-653835676 and on Yellow Submarine diffractometer at the Budapest neutron center (Hungary), experiment CERIC_20217127. The magnitude of the scattering vector q is defined as $q = (4\pi/\lambda)\sin(\theta/2)$ with θ being the scattering angle and λ the incident X-ray wavelength. SANS measurements were carried out in the q-range between 0.4–4.0 nm^{-1}, with a fixed value of the incident wavelength ($\lambda = 0.488$ nm, $\Delta\lambda/\lambda = 20\%$) and two sample-to-detector distances (1.1 and 5.2 m). The measurements were conducted at room temperature of 20°C. Samples were loaded in quartz cells of 2 mm thickness (Hellma analytics GmbH & Co. KG, Müllheim, Germany). To obtain the intensity of scattering in absolute units, a standard procedure of calibration to water was performed after subtracting the background and scattering in the solvent (D_2O) which were measured in separate experiments.

SAXS measurements were performed using polycarbonate capillaries of 2 mm thickness (ENKI, Concesio, Italy) as sample containers. The measured two-dimensional SAXS patterns were corrected for detector artefacts, normalized to absolute intensity scale and azimuthally averaged to obtain the intensity profile I(q) as a function of q, in the range ($0.7\ nm^{-1} < q < 6 nm^{-1}$). Spectra were recorded at several positions of the capillary's length to test radiation damage that might be induced by X-ray exposure. For each static measurement, at least 5 spectra were averaged after excluding any possible radiation damage. The averaged background signal was subtracted from each averaged sample intensity profile.

The analysis of the I(q) profiles was performed assuming that for a monodisperse homogeneous micellar solution as $I(q) = NV^2 2\Delta\rho^2 P(q)S(q)$ where N is the number of particles per unit volume V, $\Delta\rho$ is the contrast term between the particles and the medium. P(q) is the form factor of the micelles, giving information on their size and shape, while S(q) is the solution structure factor, that depends on the spatial distribution of interacting micelles, becoming constant, $S(q) = 1$, for dilute solutions of non-interacting micelles (Ghezzi et al., 2021).

The mucin–micelle interaction was investigated by observing the diffusion of CSA-loaded micellar solution (40 μL) put in contact with mucin (20 μL, c = 15% w/v) in the polycarbonate capillary placed in a horizontal sample holder. SAXS intensities at different positions in the capillary were measured. SNES was used as buffer for both micelles and mucin solution. Spectra of the solution in different horizontal position have been acquired over time, thus monitoring the evolution of the diffusion of the particles the first acquirable measurement, at t=200 seconds, to t=1500 seconds. As a reference, the diffusion of SNES alone in mucin has been measured.

2.2.3. Ex vivo mucoadhesion study

The mucoadhesive properties of the micelles subjected to a constant Simulated Nasal Electrolyte Solution (SNES) flow were investigated exploiting the rabbit nasal mucosa by means of an "inclined plane apparatus". The apparatus consisted of an inclined plane with an angle of inclination of 45° on which a glass Petri dish was located and used to

position the tissue and collect samples. With this test, the mucoadhesive properties of the HL micelles were investigated and compared to those of a CSA suspension (0.5 mg/mL).

The Simulated Nasal Electrolyte Solution (SNES) consisted in an aqueous solution containing calcium, sodium and potassium ions at the same concentrations present in the human nasal fluid (Eichner et al., 1983; Mahajan and Gattani, 2009). It was prepared by dissolving sodium chloride (8.77 mg/mL), potassium chloride (2.98 mg/mL) and calcium Chloride (0.45 mg/mL) in ultrapure water (Castile et al., 2013). After the complete dissolution of the salts, the pH was adjusted to 6.5 with hydrochloric acid 1M.

The nasal mucous membranes were isolated from fresh rabbit heads kindly provided by Bertoni Carni S.r.l. (Busana, Reggio-Emilia, Italy), stored in ice, and used within four hours from animal death. The heads were sectioned longitudinally, then the whole mucosa and the respective portion of supporting cartilage were taken using a scalpel. Successively, the mucosa was punched to obtain 8 mm diameter circular portions of tissue. The tissue was then placed on absorbent paper soaked in physiological solution in a closed plastic Petri before testing. During the experiment, the nasal tissue, the inclined plane apparatus and the SNES were kept at room temperature.

The mucosal tissue was fixed with the double-sided tape (Tesafix® 4934, KaiserKraft, Stuttgart, Germany) within the glass Petri dish on a horizontal plane and treated with 20 μL of the HL micellar formulation or the CSA suspension. After 5 minutes, the Petri dish was positioned on the inclined plane apparatus so that the SNES flowed over the tissue running from its upper edge to the bottom of the Petri dish, where it could be collected for analysis. To do this, the SNES was flowed at 100 μL/min with the aid of a syringe pump (Harvard Apparatus, Holliston, USA) equipped with a plastic syringe having an internal diameter of 19 mm and a needle of 0.8 × 40 mm, conditioned for at least 15 minutes before starting the experiments. Samples were collected every 5 minutes for 30 minutes and mixed with 500 μL of mobile phase. Then, samples were centrifuged (NEYA-16R, Remi Elektrotechnik, Vasai, India) at 9,500 rpm for 10 minutes at 25°C and the supernatant was analyzed by HPLC. At the end of the thirty minutes-experiment, the drug adhered to the tissue was extracted with an extracting fluid consisting of a mixture of acetonitrile and 1% acetic acid at a volume ratio of 87:13 respectively. The tissue was kept in the extracting fluid (1 mL) overnight at ambient temperature, then was sonicated and centrifuged (NEYA-16R, Remi Elektrotechnik, Vasai, India) at 12,500 rpm for 15 minutes at 25°C; 500 μL of the supernatant were withdrawn and mixed with ultrapure water (150 μL) and finally analyzed with HPLC. Moreover, 1 mL of acetonitrile was used to collect and dissolve the drug that had eventually adhered to the Petri dish; the samples were centrifuged at 9,500 rpm for 10 minutes at 25°C and the supernatant was collected and analyzed by HPLC in triplicate. The percentage of mucoadhesion was calculated considering the theoretical amount of drug deposited on the nasal mucosa as 100%, from which a cumulative curve was built by subtracting the drug amount found in the withdrawal at each time point.

Finally, a mucosal mean residence time (mMRT) was calculated from data applying Equation 1 (Clementino et al., 2021), obtained from a classic method for the calculation of the mean residence time in pharmacokinetics reported in literature (Munda et al., 1988).

$$\mathrm{mMRT} = \frac{\mathrm{AUMC}_{0\to\infty}}{\mathrm{AUC}_{0\to\infty}} \quad (1)$$

In Equation 1 reported above, AUC is the area under the curve describing the percentage of residual CSA adhering to the nasal mucosa over time, while AUMC is the area under the first moment curve. The AUC and AUMC were calculated by the trapezoidal method with exponential extrapolation, and these were used to calculate the mMRT.

2.2.4. *In vitro studies*

2.2.4.7. Cell line and culture conditions. Vero E6 cell cultures (American Type Culture Collection, ATCC CRL-1586) were grown in Minimum Essential Medium (MEM) supplemented with L-glutamine (2 mM), penicillin (100 U/mL), streptomycin (100 μg/mL) (complete culture medium) and heat inactivated fetal bovine serum (FBS) (10% v/v), as recommended. (Ammerman et al., 2008) Cells were incubated at 37°C in a humidified, 5% CO_2 atmosphere-enriched chamber until use. For compound treatment studies, cells were seeded in 96-well plates and cultured in MEM containing FBS (2% v/v). Cell culture medium and supplements were all purchased from EuroClone (Milan, Italy).

2.2.5. *Antiviral Activity Studies*

2.2.5.8. Virus propagation and titration. The inhibitory effect of pure CSA, blank and CSA-loaded micelles on viral replication was tested against Omicron subvariant BA.1, technically referred to as lineage B.1.1.529.BA.1. The viral strain was isolated from a residual clinical specimen conferred to the Unit of Microbiology, Greater Romagna Area Hub Laboratory (Cesena, Italy), for routine diagnostic purposes and sequenced as part of the project for monitoring the prevalence and distribution of SARS-CoV-2 variants in Italy, promoted by the Italian National Institute of Public Health (ISS, Rome, Italy). Before being used for this study, the sample underwent an anonymization procedure, in order to adhere to the regulations issued by the local Ethical Board (AVR-PPC P09, rev.2; based on Burnett *et al.* (Burnett et al., 2007)). In brief, a specific volume of clinical specimen (500 μL) was used to infect a cell monolayer at confluency. After a one-hour adsorption, the culture was maintained in FBS MEM (2% v/v) and incubated for 72 hours. Both the original clinical samples and the viral strains were analysed employing the FilmArray Respiratory Panel (Biomerieux, Marcy l'Etoile, France), testing negative for other respiratory viruses. After isolation on Vero E6 cells, the viral strain was in turn sequenced using CleanPlex SARS-CoV-2 Flex (Paragon Genomics, Inc., Hayward, CA, USA) and Illumina MiSeq (Illumina Inc., San Diego, CA, USA) (Genomics, n.d.) to reconfirm the lineage identification provided for diagnostic purposes. Sequenced reads were aligned and compared with the reference genomic sequence of SARS-CoV-2 Wuhan-Hu-1 isolate (Access: NC_045512, Version: NC_045512.2) using SOPHiA DDM platform software (SOPHiA Genetics, Lausanne, Switzerland), for determination of the consensus sequence, variant calling and lineage assignment.

The viral strain was titrated using the endpoint dilution method (Lei et al., 2020). In brief, serial 10-fold dilutions (from 10^{-1} to 10^{-10}) in FBS MEM (2% v/v) were used to infect confluent monolayers of cells in a 96-well plate. After 72 hours cells were fixed and stained by means of a formaldehyde solution (4% v/v) in crystal violet. Absence or presence of cytopathic effect at each dilution was assessed by comparison of each well with virus control and cell control wells. Viral titres, expressed ad $TCID_{50}$/mL, were calculated with the Reed and Muench formula based on eight replicated for dilution (Reed and Muench, 1938).

2.2.5.9. Cell treatment and viral replication inhibition assay. The day prior to treatment and infection, Vero E6 cells were seeded at a density of 2×10^6 cells per plate in 96-well plates and allowed to attach for 16 to 24 hours at 37°C, 5% CO_2. On the day of infection, each tested compound stock solution was freshly diluted in cell culture medium containing FBS (2% v/v). CSA was tested at concentrations ranging from 2 μM to 64 μM (2, 4, 8, 16, 32 and 64 μM) (de Wilde et al., 2011). Each CSA-loaded micellar formulation was diluted accordingly, in order to obtain the same CSA concentrations. Similarly, the blank micelles were diluted to obtain the same concentration of TPGS micelles as the drug-loaded samples. In order to better determine at which level the viral replication cycle was inhibited, cells were subjected to different treatment regimens, which can be distinguished into single- and multiple-treatment regimens. The first category includes: pre-treatment 1 hour before infection (*protocol A*), simultaneous treatment and infection (*protocol B*), treatment 2 hours post-infection (*protocol C2*) and

treatment 6 hours post-infection (*protocol C6*). The second category, on the other hand, includes: pre-treatment 1 hours before infection followed by treatment 2 hours post-infection treatment (*protocol D*), three treatments post-infection (*protocol E*) and pre-treatment 1 hour before infection followed by three treatments post-infection (*protocol F*). In any case, each treatment lasted one hour and in the multi-treatment regimens, treatments were repeated one hour apart. Antiviral efficacy was tested against two different virus concentrations: 0.005 m.o.i. (*i.e.,* multiplicity of infection) and 0.0005 m.o.i. In both cases, infected cultures were incubated for one hour at 37°C to allow viral adsorption. Treated and infected cultures were incubated at 37°C, 5% CO_2 for 72 hours. For each treatment protocol, a cell culture was infected directly with the virus suspension at the two tested concentrations to assess viral replication in the absence of any potential inhibition.

2.2.5.10. SARS-CoV-2 nucleic acid quantification. Viral replication in treated and untreated cell cultures was evaluated by qRT-PCR by comparing the Ct values of each treated sample and its corresponding untreated control obtained after 72 hours of incubation. For this purpose, the Allplex SARS-CoV-2 Extraction-Free system (Seegene Inc., Seoul, South Korea) was used (Seegene Inc., n.d.). It consists of a real-time qRT-PCR multiplex assay based on the use of TaqMan probes, which allows the simultaneous detection of four target genes, namely E gene, RdRP/S gene and N gene. Sample preparation, reaction setup and analysis were performed accordingly to the manufacturer instructions. Briefly, 15 μL of the sample was diluted 1:4 in 45 μL of RNAse-free water in a 96-well PCR plate and hence an exact volume of the dilution (5 μL) was transferred to another plate with 16 μL of PCR master mix, containing the following compounds: 5 μL of MOM (MuDT Oligo Mixture, with dNTPs, oligos, primers and TaqMan 5' fluorophore/3' Black Hole Quencher probes), 5 μL of enzymes, 5 μL of RNase-free water and 1 μL of an exogenous internal control for every reaction. A positive and a negative control were included in each run. The assay was run on a CFX96 real-time thermal cycler (Bio-Rad, Feldkirchen, Germany). The amplification process includes cDNA denaturation at 95°C for 10 seconds, primers annealing at 60°C for 15 seconds and elongation at 72°C for 10 seconds (44 cycles). Fluorescent signals were acquired after every amplification cycle. Results analysis and targets quantification were performed with 2019-nCoV Viewer from Seegene Inc. (Seoul, South Korea). By comparing the Ct values referred to the N gene of each treated sample and its corresponding untreated control, the percentage of infectivity reduction was calculated as follows (Equation 2), approximating 100% of infectivity reduction to treated sample Ct value at time 0 and 0% of infectivity reduction to the Ct value obtained from the untreated controls:

$$\text{Viral infectivity reduction } (\%) = \frac{\text{Treated sample Ct value 72h} - \text{Untreated control Ct value 72h}}{\text{Treated sample Ct value t} = 0 - \text{Untreated control Ct value 72h}} \cdot 100 \quad (2)$$

2.2.6. Cytotoxicity study

Cells treated with the same treatment protocols described in Section 2.2.5 but not infected were used to assess cytotoxicity. For this purpose, the blank and drug-loaded micellar formulations (HL, ML, LL; diluted to a CSA concentration in the range of 2-64 μM) as well as the pure CSA powder (2-64 μM) were tested.

To quantify cell viability, after the incubation period, the cell monolayers were fixed and stained using a 4% formaldehyde solution in crystal-violet; absorbance was read at 595 nm. For each tested compound concentration, the percentage of viable cell for each tested concentration was calculated, setting the mean absorbance value of the cell control wells (neither treated, nor infected cells) as 100% viability. The tested formulation and relative dilutions were considered cytotoxic when lead to a cell viability lower than 80%.

2.2.7. Spray characterization

Three different nasal devices were provided by Aptar Pharma (Le Vaudreuil, France) and used for spray characterization and deposition in the nasal cast assessment: an amber glass vial equipped with CPS preservative-free spray pump, 70 μL/single spray (device A), a Bidose system BDSI V3 device, 100 μL/single spray (device B) and a BiVax system, 250 μL/single spray (device C) assembled using a standard kit BDSI (references 2457_010 et 2457_140) (Figure S1, Supplementary Material). While device A was a multi-dose nasal spray, on the other hand device B and device C were able to administer only two consecutive doses of the formulation.

Droplet Size Distribution (DSD) of the aerosol emitted from the selected devices was carried out employing Malvern Spraytec (Malvern Panalytical Ltd, Malvern, UK) in open bench configuration. The nasal spray was actuated at 3 cm and 6 cm with the plume cutting perpendicularly the laser beam. Data collected were analyzed in terms of transmittance, volume diameter of the 10^{th}, 50^{th} and 90^{th} percentile of the distribution and width of the droplets distribution obtained (span). Three replicates per distance for each device were performed.

The plume of the formulation sprayed from the selected pump was characterized also employing a pulsed laser technique using Patternate software version 1.3.1 (Oxford Lasers, Didcot, UK).

For Spray Pattern (SP) the laser beam was positioned at 3 cm and 6 cm from the pump nozzle. The laser cut the plume horizontally whilst high-speed images were recorded. SP allowed to collect the following spray characterization parameters: minimum diameter (Dmin), maximum diameter (Dmax), ovality ratio ($\frac{Dmax}{Dmin}$) and area ($\pi \times \frac{Dmin}{2} \times \frac{Dmax}{2}$). Three replicates per distance for each device were performed.

For Plume Geometry (PG) the laser beam was positioned at a distance to allow for the capture of the whole plume emitted from the device nozzle. The laser beam cut vertically the plume while high-speed images were recorded. PG allowed to analyze the following parameters: plume angle (°), plume length (cm) and plume width (cm). The plume width was taken at a plume length of 6 cm. Three replicates per device were carried out for PG.

The screened nasal devices were automated actuated for spray characterization employing Vereo® actuator (NSx, Proveris Scientific Corporation, MA, USA). The method for automated actuation employed was previously developed and validated by Aptar Pharma (Table S1, Supplementary Material).

2.2.8. Deposition study on a nasal cast

The deposition profile of the developed micelles was studied using a silicone nasal cavity model by Koken® (Model LM-005 Koken ltd., Tokyo, Japan) (Figure S2, Supplementary Material).

For these studies, as for the mucoadhesion studies, the micellar formulation with the highest drug content (HL micelles) was selected since it was considered the best candidate for a possible *in vivo* administration.

For each kind of device (Figure S1, Supplementary Material), the experiments were performed in triplicate. The experiments were performed in absence of any simulated inhalation flow, and each device was actuated once into the left nostril at a 45° angle considering the palate as reference.

Device **A** was filled with 5 mL of micellar formulation, primed four times before the analysis, and inserted 12 mm into the nostril. Device **B** was filled with 250 μL of micellar formulation and inserted 7 mm into the nostril without being primed, according to the manufacturer instructions. Device **C** was filled with 300 μL of micellar formulation, primed once according to the manufacturer and inserted 7 mm into the nostril. In order to identify the areas in which the micellar formulation was deposited, we used for each analysis about 0.6 g of the color finding past Sargel® (Arkema, Exton, PA, U.S.A), which in contact with the water present in the formulation becomes pink (Kundoor and Dalby, 2011).

A digital camera equipped with a 16-50 mm lens (Sony α 5100, Sony, Tokyo, Japan; 24.3 megapixels APS-C sensor) was used to capture the images, keeping the nasal cast 15 cm apart from the camera; to standardize photographic conditions a photographic set was used with a white background and the same light condition for all the pictures. To balance the ambient light, the experiments were performed in a dark room, using a LED light as the only light source, kept at a fixed distance from the nasal cast. The positions and distance between the camera and the cast were maintained fixed. The camera was set with an exposure time of 1/250 s, the ratio of focal length to effective aperture diameter (f) was 4.5, with a focal distance of 16 mm and ISO 250. For each analysis, 1 minute elapsed between the actuation of the device and the imaging. Each device was weighed before and after each actuation in order to know how much formulation was dispensed.

The pictures were elaborated using the ImageJ software (U.S. National Institute of Health, Bethesda, MD, USA) to analyze the deposition area and identify the deposition regions. For this purpose, the nasal cavity was divided into four regions of interest (ROI): the vestibule, the middle-upper turbinate, the lower turbinate and the throat (Figure S2, Supplementary material). The images acquired one minute after spraying were converted to an 8-bit color image and the conversion of the number of pixels into mm^2 was realized by using a graduated scale positioned near the nasal cast during the analysis. The threshold level range was fixed between 0 and 109 for all the acquired images.

2.2.9. Statistical Analysis

Differences were analyzed using one-way ANOVA and Tukey HSD Post Hoc test (α=0.05) using KaleidaGraph software (ver. 4.5, Synergy Software, Reading, PA, USA) and were considered statistically significant when $p < 0.05$.

3. Results

3.1. Characterization of the blank and CSA-loaded micelles

As shown in Table 1, all the produced micelles showed a particle size below 15 nm, low values of polydispersity index (PDI) and an almost neutral surface. The density of the micellar formulation was in all the cases slightly above the value of 1 g/cm^3, with a tendency to slightly increase with increasing CSA loading. The CSA-loading encapsulation efficiency for low-loading (LL, 0.1 mg/mL), medium-loading (ML, 0.25 mg/mL) and high-loading (HL, 0.5 mg/mL) CSA micelles was in all cases higher than 95% without statistically significant differences. Despite showing the rheological behavior of a dilatant fluid (shear thickening), at low shear the viscosity calculated at 25°C was basically the same for all the developed micelles, turning out to be slightly above 1 mPa·s. No differences were found between the blank and the three types of CSA-loaded micelles, and the amount of CSA present in the formulations does not seem to have any impact on the viscosity. The viscosity of the micelles was also analyzed at 37°C to simulate the nasal environment, but again no differences were evidenced apart the expected slight decrease in viscosity values. The viscosity flow curves of the micellar formulation at 25°C and at 37°C are reported in Supplementary Material (Figure S3). The pH of the blank and the HL micelles turned out to be similar; more precisely, it was 4.56 ± 0.03 and 4.81 ± 0.01 respectively. The pH of the ML and LL micelles was higher; more precisely, it was 6.65 ± 0.01 and 6.42 ± 0.03 respectively.

The presence of CSA in the micellar structure appears to slightly but consistently reduce their average hydrodynamic radius of around 10% compared to the value of blank micelles (Table 1). The results of the characterization made on the micellar formulation over 7 months after the first characterization are collected in Supplementary Material Table S2.

A structural analysis of micelles was performed by Small Angle Neutron Scattering (SANS) performing experiments on both blank and CSA-loaded micellar formulations. The intensity spectra measured at room temperature are reported in Fig. 1. The background-subtracted scattered intensity I(q) can be expressed as Equation 3:

$$I(q) = NV^2 2\Delta\rho^2 P(q)S(q) \quad (3)$$

where N is the number of particles per unit volume V, $\Delta\rho$ is the contrast term between the particles and the medium, P(q) and S(q) are the particle form factor and the structure factor, describing the size, the shape and interactions between particles, respectively. Fig. 1**A** reports the intensity spectra of blank micelles along a dilution line (TPGS concentration from 30 mg/mL to 1.5 mg/mL, *i.e.* up to 1:20 dilution), to verify the stability of the micelles and to enucleate information on the particles' size and shape. The features of SANS curves are similar, although a depression of the intensity profile in the low-q region is visible in high concentration samples. This trend is characteristic for interacting particles, experiencing steric repulsions, which vanish at low concentration. In the non-interacting regime (concentration below 6 mg/mL) the intensity curves are superimposable, indicating that micelles are physically stable, with identical size and shape. Structural details were obtained fitting the curves to a core−shell sphere model combined with a hard-sphere structure factor, as already reported in the literature for TPGS micelles (Puig-Rigall et al., 2017). The fit is reported for the sample diluted 1:20 (1.5 mg/mL) in Fig. 1**A** and the parameters are reported in the **Supplementary Material**. Micelles display a hydrophobic core of 7 nm (diameter) surrounded by a hydrophilic shell with a thickness of 2.9 nm. The calculated overall size of the micelles, around 13 nm, is in good agreement with DLS data. The amphiphilic nature of TPGS leads in water to the formation of a micellar structure composed of an inner lipophilic core encapsulating the lipophilic drug and responsible for its solubilization, and an outer hydrophilic shell involved in the interaction with the biological surfaces upon administration (Ghezzi et al., 2022).

Interestingly, the addition of cyclosporine A results in an increase of inter-particle interaction. In fact, the intensity profile at low q lowers

Table 1
Physico-chemical characterization of blank and 0.1, 0.25, 0.5 mg/mL CSA-loaded micelles at time 0 (n=3).

	Size [nm]	PDI	Zeta Potential [mV]	Density [g/cm^3]	Encapsulation Efficiency [%]	Viscosity (25°C) [mPa·s]
Blank	13.2 ± 3.2	0.08	-2 ± 0	1.0061012 §	–	1.24 ± 0.06
LL micelles (0.1 mg/mL)	11.7 ± 0.5	0.07	-2 ± 1	1.0061056 §	99.49 ± 8.37	1.26 ± 0.07
ML micelles (0.25 mg/mL)	11.4 ± 0.1	0.06	-1 ± 1	1.0061630 §	98.15 ± 5.60	1.27 ± 0.06
HL micelles (0.5 mg/mL)	11.7 ± 0.2	0.12	-1 ± 1	1.0062672 §	97.40 ± 2.69	1.25 ± 0.07

§ the SD of the results is below 0.000005.

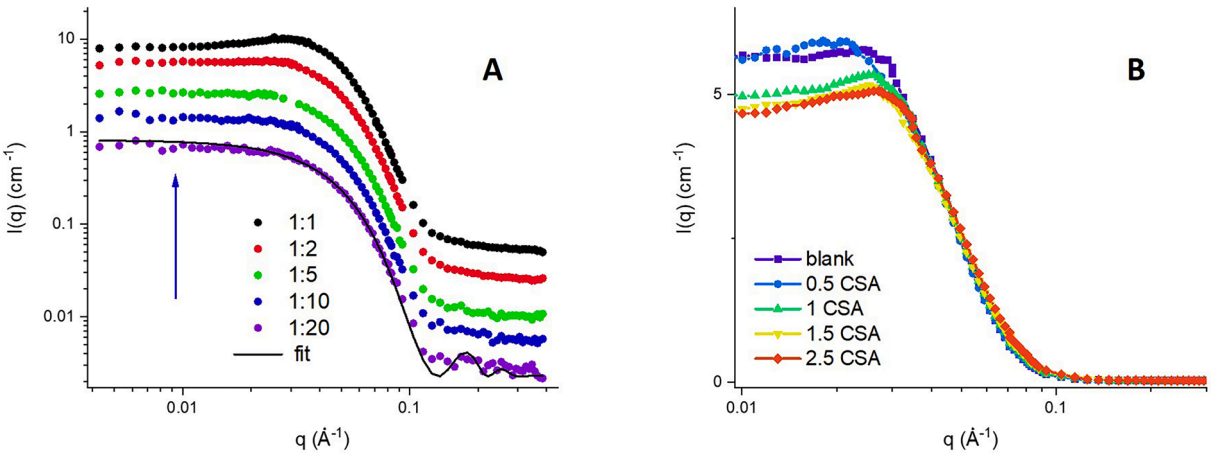

Fig. 1. SANS spectra of micelles at room temperature. A) blank micelles at different dilution, starting from 30 mg/mL w/v. The fit of the most diluted system is reported (black solid line). B) micelles (15 mg/mL), at different CSA loading, as reported in the legend (CSA concentrations in mg/mL). The intensity is reported in linear scale to highlight the effect of the structure factor in the low q region.

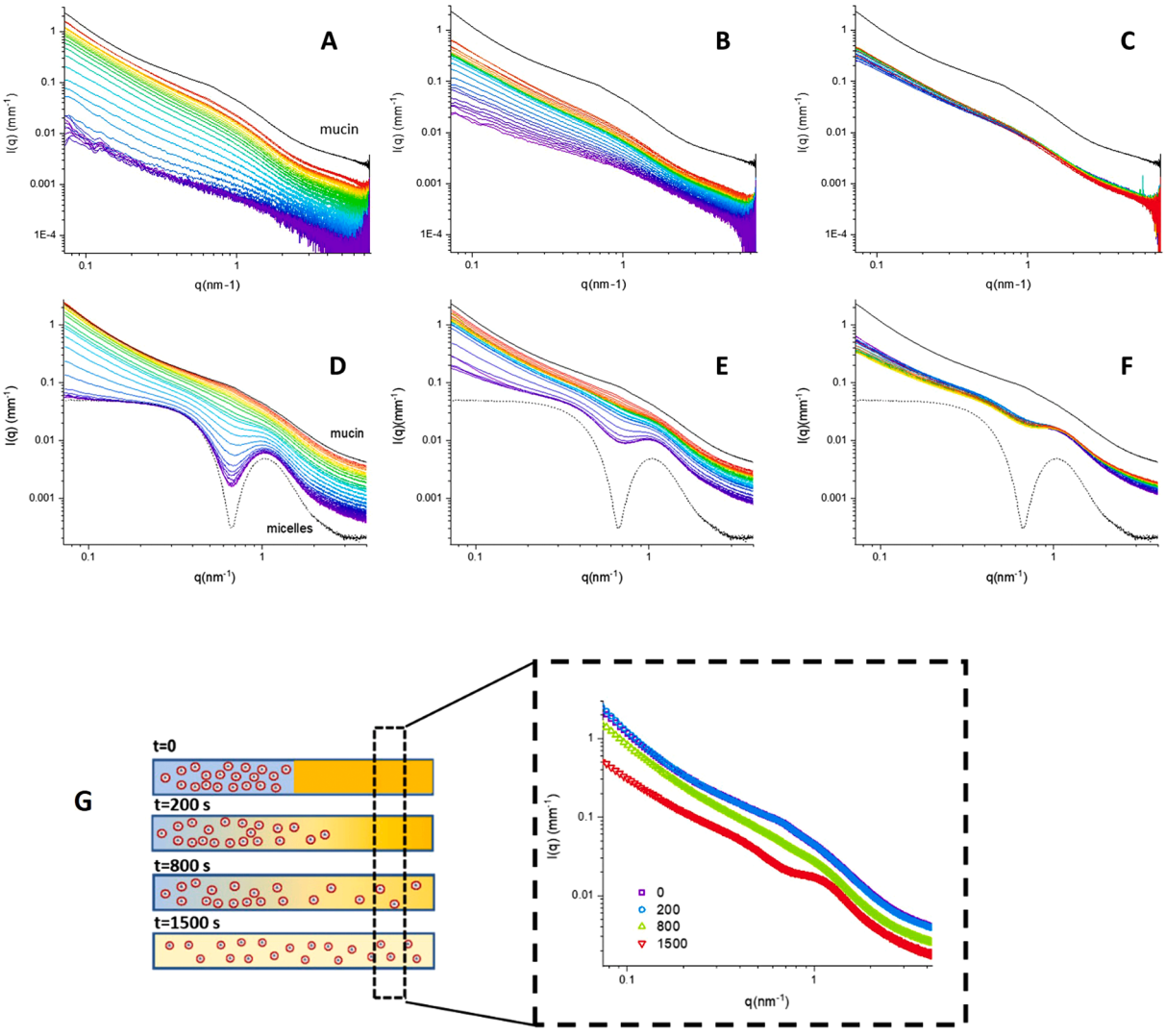

Fig. 2. A-C) SNES diffusion in mucin during time. SAXS spectra at different positions in the horizontal capillary at three delays (from left to right: 200, 800, 1500 s). D-F) Micelles diffusion in mucin. SAXS spectra of micelles at different positions in the horizontal capillary at three delays (from left to right: 200, 800, 1500 s). G) sketch of the experimental set up and time evolution of the SAXS spectra acquired at 2.4 mm distance from the mucin/micelles contact interface (as indicated by the dotted square) over time (from t=0 to t=1500 s).

accordingly to the amount of loaded CSA, as shown in Fig. 1**B**. This increase of steric repulsion between micelles at a constant solution concentration indicates that micelles become closer and more numerous, *i.e.* smaller. As for blank micelles, SANS curves of CSA-loaded micelles were fitted to a core−shell sphere model combined with a hard-sphere structure factor (Puig-Rigall et al., 2017) and results are reported in **Supplementary Material**. In agreement with DLS data, results indicate an overall reduction of the size of the CSA-loaded micelles. Analysis of the SANS spectra reveals that the size of the micelle core decreases from 7 to 6.4 nm, while the hydrophilic shell keeps a constant thickness (2.9 nm).

3.2. SAXS mucodiffusion study

The stability of the micellar structure when in contact with mucus and the propensity of micelles to permeate and cross a mucus layer were investigated by SAXS, observing the interaction of micelles with mucin. Mixed mucin-micelles samples were prepared by mixing 40 μL of HL micelles formulation (30 mg/mL) with 20 μL of a mucin type II solution 5% w/v. The scattered intensity profiles of the mixed samples, reported in **Supplementary Material**, can be reconstructed by the mere sum of the intensity contribution of micelles and mucin, revealing that the micelles are stable in the glycoprotein network and do not interact with mucin.

The propensity of the micelles to penetrate into a mucus layer after contact was investigated by observing the diffusion process of the micelles in a layer of mucin, as sketched in Fig. 2**G**, exploiting the shorter acquisition time of SAXS measurements (1 s) with respect to SANS (2.5 hours).

For these diffusion experiments, an already published protocol was used (Di Cola et al., 2019): 40 μL of HL micelles formulation (30 mg/mL) were carefully put in contact with 20 μL porcine mucin (15% w/v) in a polycarbonate capillary (2 mm diameter), placed in a horizontal sample holder. SAXS intensities at different positions in the capillary were measured at different time delays (200, 800 and 1500 seconds). Results obtained for Simulated Nasal Electrolyte Solution (SNES) alone and CSA-loaded micelles are reported in Fig. 2. The graphs (Fig. 2 **A-C**, SNES in mucin and Fig. 2 **D-F**, micelles in mucin) represent the evolution of the systems over time, after 200, 800 and 1500 s. The red curves are acquired in the mucin section of the capillary, as can be confirmed by the similarities with the pure mucin curve (reported in black on top) while blue curves represent the spectra acquired in the SNES or micelles section. The spectrum of pure micelles, is reported for comparison, presenting intensity minima and maxima (black line on the bottom of the graphs, **D-F**). The mixing kinetic of the two samples is appreciable, from a state in which the two main components, *i.e.* mucins and SNES or micelles, are clearly separated (Panel **A, D**) to the final state in which components are homogeneously mixed (Panel **C, F**).

To highlight the effective micelles permeation into the mucus, spectra acquired at a fixed position (2.4 mm from the samples contact interface) in the mucin section are reported in Fig. 2**G** at different delays. The transition from a mucin-like spectrum toward a mixed micelle-mucin spectrum is clearly visible. This indicates the ability of the micelles to enter easily into mucin (15% w/v concentration). A similar behaviour has been observed for the diffusion of a sample of SNES alone into mucin, as reported in **Supplementary Material**. Results indicate that micelles are able to enter and percolate together with water into mucin, with a diffusion time of the order of 10 μm/s, comparable with the one observed using SNES alone.

3.3. Ex vivo mucoadhesion study

The HL micelles were compared to a CSA suspension for the tendency to adhere to the nasal tissue exploiting an excised rabbit mucosa positioned on an inclined plane apparatus.

The HL micelles resulted significatively less bioadhesive than the water suspension of CSA at the same concentration, used as control. After 30 minutes indeed, it has been shown that only 26% of the CSA belonging to the micellar formulation adhered to the fresh rabbit mucosa. As can be seen from Fig. 3, most of the micellar formulation deposited on the nasal mucosa was removed already during the first 5 minutes of the experiment, with a dramatic fall in percentage of CSA adhering to the nasal mucosa. Then, from 5 to 30 minutes, the percentage of CSA adhering to the mucosa decreased very slowly.

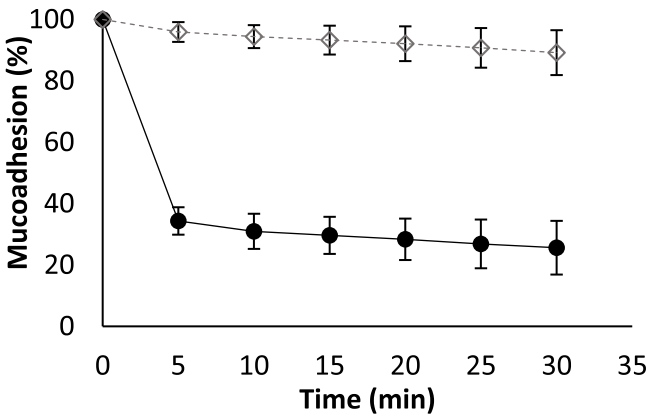

Fig. 3. Ex vivo mucoadhesion study on rabbit's nasal mucosa. Comparison between the mucoadhesive properties exhibited by the micelles loaded with 0.5 mg/mL CSA (black circles) and those exhibited by a 0.5 mg/mL CSA suspension (gray empty diamonds) used as reference. (n=6).

The 0.5 mg/mL CSA suspension showed a different behavior, demonstrating to be more mucoadhesive than the micellar suspension, as can be seen from Fig. 3. In this case, 89% of the drug initially deposited on the mucosa adhered to the tissue even after 30 minutes. Exploiting the collected data, the mucosal mean residence time (mMRT) was calculated for both the micellar formulation and the drug suspension. The mMRT of the micelles turned out to be significatively lower than that of the drug suspension. More precisely, the micellar mMRT was 42.9 ± 8.8 minutes, while the mMRT of the drug suspension was 163.8 ± 28.6 minutes.

3.4. Cytotoxicity study on Vero E6 cells

The cell viability of the Vero E6 cell cultures treated with CSA alone was completely comparable to that of the untreated ones, so none of the pure CSA concentration tested proved to be cytotoxic for Vero E6 cells. The LL micelles appeared extremely cytotoxic at the three upper concentrations tested, *i.e.* 16 μM, 32 μM and 64 μM containing respectively 3.81 mM, 7.63 mM and 15.25 mM TPGS. The same cytotoxicity profile was demonstrated for the blank micelles at the corresponding TPGS concentrations.

Similarly, the ML micelles were cytotoxic at the tested CSA concentrations of 32 μM and 64 μM (TPGS concentration: 3.05 and 6.10 mM respectively). Finally, as regards the HL micelles, only the CSA concentration of 64 μM (15.25 mM TPGS) provoked cytotoxicity.

In all the experiments, the same cytotoxicity profile was demonstrated when testing the blank micelles at the TPGS concentrations corresponding to the CSA-loaded formulations, indicating that the surfactant is the component responsible for the observed toxicity.

3.5. Antiviral activity of the developed micelles against SARS-CoV-2

The ability of the CSA-loaded micelles to prevent and/or block SARS-CoV-2 replication was tested *in vitro* on Vero E6 cells and compared to the antiviral activity of both CSA solution and blank micelles. Cytotoxic formulations, *i.e.* those that reduced the cell viability below 80%, were excluded from the evaluation. Cells were treated following different

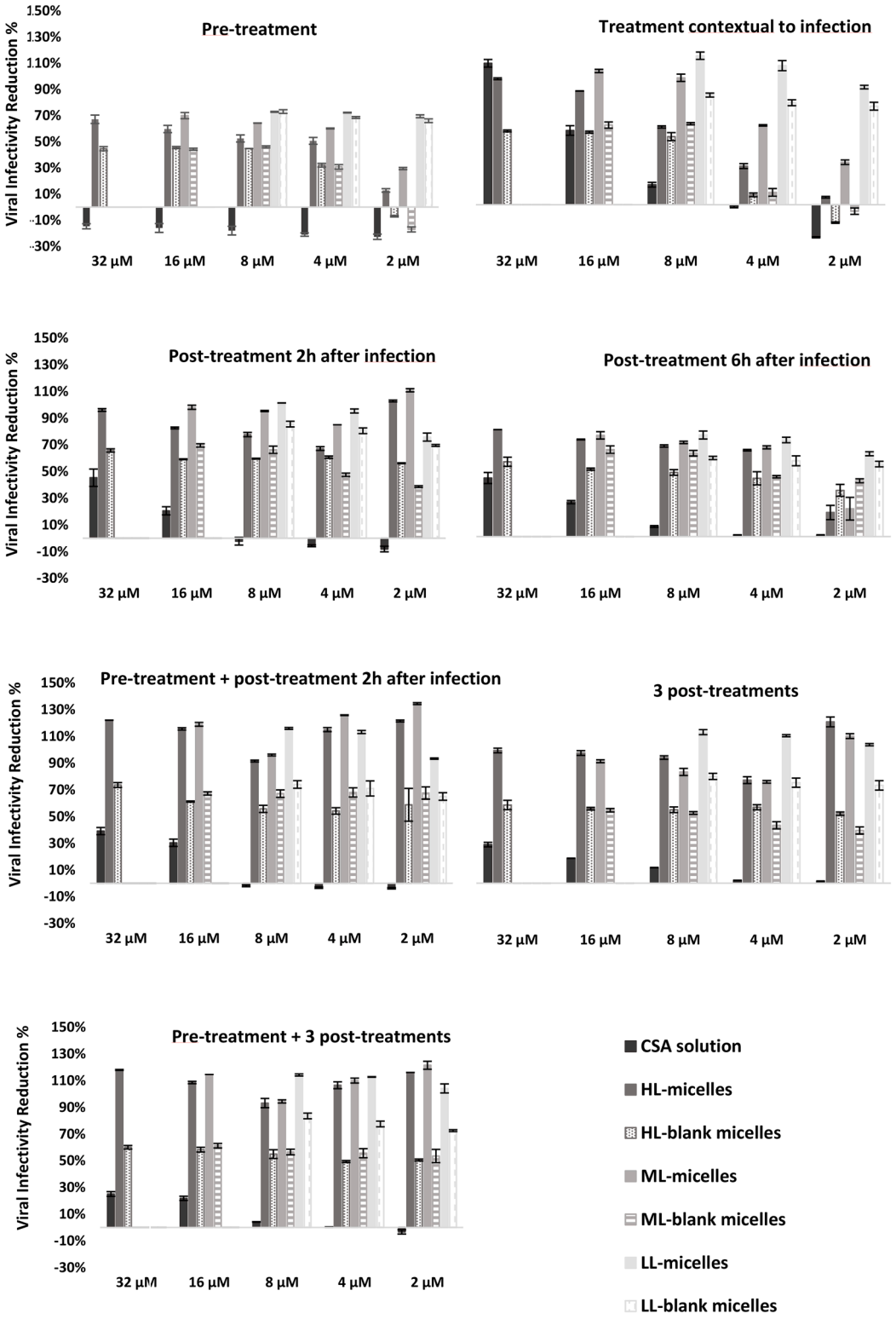

Fig. 4. - Antiviral activity of the HL micelles, ML micelles and LL micelles compared to the raw CSA and the blank formulations. Each graph represents the results obtained by treating the infected cells with one of the seven different protocols tested: treatment 1h before infection (protocol A), treatment contextual to the infection (protocol B), post-treatment 2h after the infection (protocol C), post-treatment 6h after the infection (protocol C6), pre-treatment 1h before the infection followed by a post-treatment 2h after the infection (protocol D), 3 post-treatments spaced 1h apart (protocol E), pre-treatment 1h before the infection followed by 3 post-treatments spaced 1h apart (protocol F).

protocols, based on different treatment timing (pretreatment, treatment contextual to the infection, post-treatment 2 hours or 6 hours after the infection) and treatment repetitions (single or multiple treatments). This approach was aimed at understanding which stage of viral replication is targeted by CSA and which is the most advantageous mode of administration of micelles in view of a possible *in vivo* intranasal administration.

As shown in Fig. 4, we found that, overall, the CSA-loaded micelles performed significatively better than both CSA solution and the blank micelles, attaining in most cases a percentage of viral inhibition higher than 100%. The results obtained by working with two different viral loads, *i.e.* 0.005 and 0.0005 m.o.i. (multiplicity of infection, *i.e.* the ratio of the number of virus particles to the number of target cells) were in good agreement even if the efficiency of the drug-loaded micelles turned out to be higher when a lower viral amount was used, as expected. Here below, we present the results obtained working with 0.005 m.o.i. while Supplementary Material contains a comment on the results obtained by treating cells with 0.0005 m.o.i. (Figure S7). Table 2 reports the concentration of TPGS in the micellar solutions tested.

In the case of the pre-treatment protocol (one hour treatment before the infection, Fig. 4**A**) both HL and ML micelles showed a maximum antiviral activity of about 70%, significatively better if compared to both CSA solution and blank micelles. Regarding the micelles with the lowest CSA loading (LL micelles), in this protocol the results obtained by using the blank and the drug loaded micelles were similar. In general, the blank micelles, used as reference, showed a variable antiviral action, with values however significantly lower than those obtained with the corresponding loaded micelles. The CSA controls, in which the drug solution was used, turned out to be ineffective against SARS-CoV-2 at all the concentrations tested.

When a treatment contextual to the infection was used (one hour treatment in presence of the virus), in most cases the loaded micelles turned out to perform significatively better than the CSA alone and the blank micelles controls (Fig. 4**B**). All the drug-loaded formulations showed a similar trend, consisting in an increasing antiviral activity with increasing CSA concentrations, leading to values above 90% of viral inhibition for HL, ML, and LL at 32, 8 and 4 μM, respectively. In particular, among all the CSA-loaded micelles, the LL formulation showed the highest antiviral activity (107%) when used at a CSA concentration of 8 μM.

CSA solution used at concentration between 2 and 16 μM were significantly less effective if compared to the loaded micelles. The CSA solution only showed an antiviral activity comparable to that of the drug-loaded micelles when applied at the highest concentration tested which was 32 μM. It must be underlined that this was the only case in which we registered a 100% antiviral efficiency for the non-formulated CSA.

The blank micelles used as reference, although showing an appreciable effect (7-79%), sometimes even higher than CSA solution, turned out to be in all the cases significantly less effective than the corresponding drug loaded micelles.

When applied post-infection (one hour treatment two hours after the infection, Fig. 4**C**), all the drug-loaded micelles turned out to be significatively more effective at hindering viral replication if compared to both the blank micelles and the CSA solution. HL and ML micelles showed a similar behavior, turning out to be more effective at the lowest CSA concentration tested, 2 μM. More precisely, the HL micelles exhibited a 102% viral inhibition, while the ML micelles exhibited a 111% viral inhibition. The LL micelles effectiveness was proportional to the CSA concentration, with a peak in correspondence of the 8 μM drug concentration (101%). When applied two hours after the infection at the highest concentration tested (corresponding to 32 μM), the CSA solution inhibited the SARS-CoV-2 replication up to 45%. A certain antiviral activity was also evidenced at a drug concentration of 16 μM, at which the viral replication was inhibited by 21%. Under this concentration, no antiviral effect was observed for the raw peptide.

Blank micelles highlighted a certain antiviral activity (38-66%) significantly lower than the drug-loaded micelles.

When a delayed treatment protocol was used (one hour treatment six hours after the infection, Fig. 4**D**), the lowest percentages of viral inhibition for all the three different developed micellar formulations were obtained (77% at 32 μM, 73% at 16 μM, 73% at 8 μM for HL, ML and LL micelles, respectively). The not-formulated CSA demonstrated a 42% viral inhibition at 32 μM, and a 25% viral inhibition at 16 μM. Its effectiveness dramatically decreased with lower concentrations becoming totally ineffective for concentrations below 8 μM. Nevertheless, in all the cases the drug-loaded micelles performed significatively better than the CSA raw material and in most cases than the blank micelles, with the only exception of CSA concentration of 2 μM, where blank micelles performed better than HL and ML micelles, but with antiviral efficacy below 40%.

When treatment was applied twice pre- and post-infection (one hour treatment before the infection and a posttreatment two hours after the infection, Fig. 4**E**), all the developed CSA-loaded micellar formulations showed significatively improved values of viral inhibition if compared to both the peptide solution and the blank micelles at all the CSA concentrations tested.

The HL and ML micelles showed a similar trend consisting of a very high antiviral activity, never going under 90%, with highest values at 2 μM (122% for HL and of 135% for ML micelles).

The behavior showed by the LL micelles was slightly different, *i.e.* consisted in a peak of activity (116%) at 8 μM but lower values at decreasing CSA concentrations, however never going under 100% inhibition. Antiviral effect of drug-loaded micelles was consistent.

The CSA showed a maximum of 39% of antiviral activity when tested at the highest concentration (32 μM), but below 16 μM no antiviral effect was observed. For all the blank formulations higher antiviral activity was detected compared to the one obtained by using the peptide solution; however, the inhibition never exceeded the value of 74%.

In the case of repeated post-treatments (one hour treatment repeated two, four and six hours after the infection, Fig. 4**F**) the developed CSA-loaded micellar formulations provided an overall performance quite similar to the previous condition. The HL and ML micelles showed high antiviral activity in all the conditions tested (never under 70%), with highest values recorded at 2 μM (109% for HL and 106% for ML micelles). The results obtained using the LL micelles were slightly different, showing the highest activity (106%) at 8 μM but lower values at decreasing CSA concentrations, however never going under 93% inhibition. Again, for CSA solution and blank micelles antiviral activity (max. 28% for CSA solution and 88% for blank micelles) was invariably lower than the one obtained for the corresponding drug-loaded micelles at all the concentrations tested.

Finally, when a pre-treatment was associated with repeated post-treatments (one hour treatment before infection and repeated treatments two, four and six hours after the infection, Fig. 4**G**) the two previous conditions data (Fig. 4**E** and 4**F**) were confirmed. Indeed, all the drug-loaded micelles performed significatively better than the non-formulated drug and the control blank formulation. The antiviral activity observed from the HL and ML micelles was again very high (always above 90%) with the highest value (116% for the HL and 121% for

Table 2
Composition of the micellar solutions used for the determination of the antiviral activity.

CSA (μM)	TPGS (mM)		
	HL	ML	LL
32	1.525	-	-
16	0.763	1.525	-
8	0.381	0.763	1.907
4	0.191	0.381	0.953
2	0.095	0.191	0.477

the ML micelles) recorded at 2 μM CSA concentration. LL micelles peak of antiviral activity (115%) was observed at the highest CSA concentration tested (8 μM). CSA solution and blank micelles antiviral activity (max. 25% for CSA solution and 84% for blank micelles controls) was lower than the one obtained for the corresponding drug-loaded micelles at all the concentrations tested. The results of the statistical analysis performed on data obtained by the *in vitro* studies are collected in Supplementary Material (Tables S4-S17).

3.6. Spray characterization

The HL formulation was loaded into three different devices, namely a conventional multidose preservative-free spray pump (CPS, device **A**) and innovative Bidose (device **B**) and BiVax (device **C**) nasal devices, to assess the potential nasal application of the micelles system developed.

Integrity of the micelles delivered by the three devices was studied employing DLS. As reported in Table 3, the BiVax device was the one which reported comparable size and PDI with the bulk formulation, whereas, particularly with the conventional spray pump, a slight increase in size and PDI was observed, indicating more polydispersity of the sample analysed with a very moderate tendency to aggregation of the sprayed micelles. A negligible increase in Zeta Potential was observed as well for all sprayed samples analysed, regardless of the nasal device employed.

The spray emitted from the three devices was then characterized in terms of droplet size distribution (DSD), spray pattern (SP) and plume geometry (PG).

DSD (Fig. 5) analysed at 3 and 6 cm from the laser beam showed comparable size for the droplets emitted by the Bidose (**B**) and BiVax (**C**) systems (mean volume diameter (D_{v50}) of 30.4 ± 1.9 μm and 34.6 ± 1.2 μm, at 3 cm respectively, and D_{v50} of 42.8 ± 2.0 μm and 42.3 ± 4.8 μm, at 6 cm respectively), whereas the CPS nasal pump (**A**) reported larger droplets (D_{v50} of 45.6 ± 0.6 μm at 3 cm and 49.1 ± 1.1 μm). Span was also higher for the droplets generated by CPS pump showing a wider droplet distribution in comparison of the other two nasal devices. This will determine a tendency of higher deposition in the anterior region of the nose for CPS nasal pump. However, the percentage of droplets below 10 μm was < 3% for all three systems employed, ideal to avoid deposition into the throat targeting just the nasal cavity, namely the primary entry and infection site of the virus.

Plume geometry (PG) and spray pattern (SP) were measured for all three devices. PG did not display any relevant difference between the spray emitted by the systems (Fig. 6). The main effect observed on the shape of the plume was correlated with the volume delivered by a single actuation of the different devices: 70 μL for the conventional spray pump, 100 μL for the Bidose and 250 μL for BiVax. The latter showed the largest plume minimum and maximum diameter by SP at both distances evaluated (Table 4), whereas the spray area increased proportionally to the volume delivered by a single shot (BiVax ≥ Bidose > CPS nasal pump). However, the effect of the spray volume was predominant for BiVax in comparison to CPS nasal pump and Bidose, which behaved more similarly.

Table 3
Integrity of the HL micelles formulation delivered by the three nasal devices.

	Size [nm]	PDI	Zeta Potential [mV]
HL micelles 0.5 mg/mL (before firing)	11.3 ± 0.1	0.08	-1.5 ± 0.2
HL micelles 0.5 mg/mL (fired by BiVax)	11.5 ± 0.1	0.08	-3.7 ± 0.3
HL micelles 0.5 mg/mL (fired by Bidose)	11.9 ± 0.1	0.20	-3.5 ± 0.9
HL micelles 0.5 mg/mL (fired by CPS spray pump)	12.2 ± 0.4	0.22	-3.8 ± 0.7

3.7. Formulation deposition in a nasal cast

The characterization studies demonstrated the high rate of mucopenetration of micelles developed in this work as well as their potential for nasal application.

The three different devices were then used to deliver the HL formulation and thus originate different deposition profiles within the nasal cavity. The study aimed to select the device most suitable for intranasal administration of micelles loaded with CSA to counteract SARS-CoV-2 infection in the upper airway.

The deposition study performed on the silicon nasal cast highlighted that the three different devices tested performed in a significantly different manner. As can be seen from Fig. 7, the BiVax System nasal atomizer (device **C**) allowed to reach the highest deposition area (45.52 ± 3.09 %) into the nasal cavity. A statistically significant lower total deposition area (32.42 ± 2.68 % and 25.85 ± 7.39 %) was obtained by using the Bidose System BDSI V3 (device **B**) and CPS spray pump (device **A**), respectively. These results were in line with the spray characterization results collected, which showed a similar spray pattern for devices **A** (CPS nasal pump) and **B** (Bidose System), in comparison to the one of BiVax (device **C**).

As illustrated in Fig. 7 below, when devices **A** and **B** were used, the micellar formulation mainly deposited in the ventral region of the nose, called *vestibulum*, and to a lower extent but in similar percentages in the middle-upper and lower turbinate. More precisely, the ratio between the deposition in the *vestibulum* and that in the middle-upper or inferior turbinate was 3:1.

On the other hand, when using device **C** (BiVax) the distribution of the administered micellar formulation appeared more homogeneously distributed on the nasal cavity surface. Indeed, the deposition was comparable between the *vestibulum*, the middle-upper turbinate and the lower turbinate. In all the three cases, the deposition at the throat level was minimal, as also observed in the DSD results, and the statistical analysis did not show any significant differences between devices **A, B** and **C**. After each spray, the behavior of the administered formulation was carefully observed, and no dripping was evidenced for the devices tested.

Moreover, the devices were weighed before and after each spray to calculate the emitted dose which in all the cases turned out to be in line with what was declared by the manufacturer. More precisely, the experimentally determined emitted dose of device A, B and C was respectively 70.00 ± 3.55 μL, 103.40 ± 13.32 μL and 236.84 ± 8.31 μL.

4. Discussion

The developed CSA-loaded micelles turned out to be perfectly in line with those already reported in literature by Pescina *et al.* (Pescina et al., 2021) and Ghezzi *et al.* (Ghezzi et al., 2022) and proposed for ocular administration, showing a particle size of ~15 nm, null surface charge and low PDI, confirming that the obtained systems were monodispersed (Stetefeld et al., 2016). The encapsulation efficiency of cyclosporine A at the concentrations tested was always nearly complete (above 97%) attesting that TPGS leads to a higher improvement of the drug encapsulation if compared to other non-ionic amphiphilic polymers, such as Solutol® HS15 and poloxamer 407. This aspect was highlighted in recent works attesting that the solubility of cyclosporine A in 20 mM TPGS is six-fold higher than that in 20 mM Solutol® HS15, (Ghezzi et al., 2022) and 8 fold higher than that in 20 mM poloxamer 407 (Pescina et al., 2019). In this work, the drug was encapsulated into the micelles at three different concentrations to evaluate whether the encapsulation efficiency could vary as the drug concentration increased. The choice to remain in the loading range between 0.1 mg/mL (equivalent to 83 μM) and 0.5 mg/mL (equivalent to 416 μM) was due to the high potency of the drug, which has proven to be effective in counteracting the replication of coronaviruses at concentrations between 2μM and 64μM (de Wilde et al., 2011).

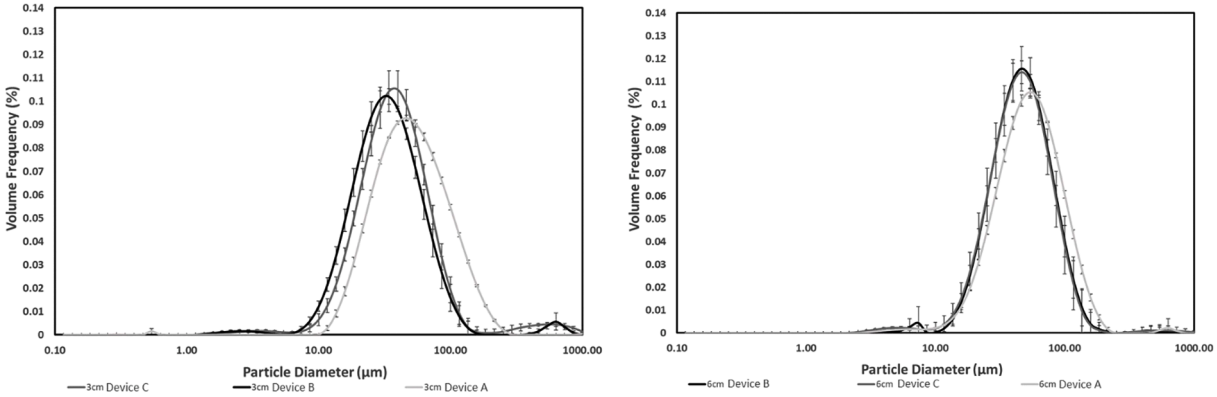

Fig. 5. DSD at 3 and 6 cm from the laser beam for the three nasal devices employed (A: CPS spray pump, B: Bidose System BDSI V3 and C: BiVax System).

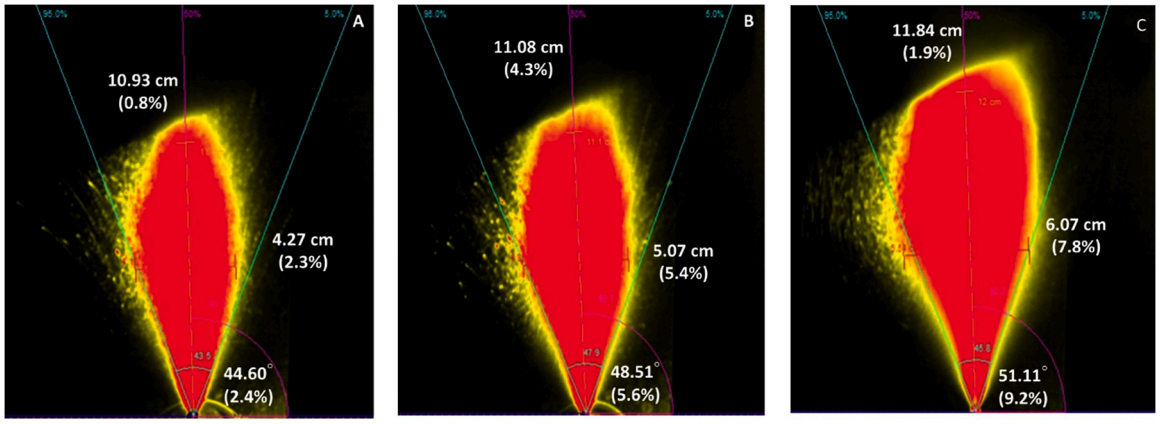

Fig. 6. PG of the spray emitted from the three nasal devices employed (A: CPS spray pump, B: Bidose System BDSI V3 and C: BiVax System).

Table 4
SP at 3 and 6 cm from the laser beam for the three nasal devices employed (A: CPS spray pump, B: Bidose System BDSI V3 and C: BiVax System).

Device	Distance	Dmin (cm)	Dmax (cm)	Ovality ratio	Area (cm^2)
CPS spray pump (A)	3 cm	2.9 ± 3.4	4.5 ± 4.1	1.6 ± 1.0	9.6 ± 6.0
	6 cm	4.1 ± 1.1	5.6 ± 5.2	1.3 ± 4.4	17.5 ± 3.3
Bidose (B)	3 cm	3.0 ± 7.8	4.7 ± 2.2	1.6 ± 9.5	9.5 ± 11.7
	6 cm	4.4 ± 11.7	6.3 ± 6.4	1.4 ± 7.8	21.6 ± 18.2
BiVax (C)	3 cm	4.0 ± 12.7	5.4 ± 4.3	1.4 ± 12.7	16.3 ± 14.5
	6 cm	6.5 ± 2.2	8.3 ± 3.6	1.3 ± 3.1	± 6.8

However, we didn't observe any decrease in terms of encapsulation efficiency with increasing drug concentration. Moreover, the amount of the drug encapsulated did not appear to have an impact on the particle size and the polydispersity index as well as on the viscosity of the formulation which was around 1 mPa·s in all the formulations at 25°C. Although it was reported in literature that the ability to encapsulate CSA within micelles of TPGS can be even 10 times that used in this work (Ghezzi et al., 2022), the drug content of our formulations was kept low, using 0.5 mg/mL as maximum concentration (except in SANS studies). This choice was motivated by the known immunosuppressive activity of CSA (Liu et al., 2020), which is obviously to be avoided when this drug is administered intranasally to have an antiviral action against SARS-CoV-2. As regards the stability, all the micelles showed a good stability profile with steady particle size, PDI and drug content during storage up to 7 months; in particular, HL micelles showed a slightly better stability if compared to the ML and LL micelles. Considering this factor as well as the fact that HL, by containing the highest drug concentration, would allow to reduce the volume to be administered potentially *in vivo*, we identified HL as the best candidate for the future *in vivo* studies, therefore decided to test only them to evaluate the mucoadhesion profile and behavior when sprayed with nasal spray.

As highlighted by SAXS and SANS analysis, the presence of CSA in the micellar core affected the size and shape of the self-aggregating micelles even in small amount (few molecules per micelle). The CSA-loaded systems rearrange, as a function of CSA loading, in micelles with a slightly smaller spherical hydrophobic core (size from 7 to 6.4 nm) surrounded by a hydrophilic shell of constant thickness (2.9 nm).

Quite interestingly, the CSA-loaded micelles formulations were demonstrated to be stable in simulated mucus, suggesting that they are not inclined to interact with mucin glycoproteins neither by electrostatic interaction nor by hydrogen bonding. This is a feature attributable to the almost neutral surface of the micelles, allowing to avoid the possible electrostatic interaction of the micelles with the negatively charged sialic acid residues characterizing the mucins (Larhed et al., 1997). Moreover, we observed a poor tendency of the micelles to stick to the mucus layer on the *ex vivo* model used, obtaining highly reproducible

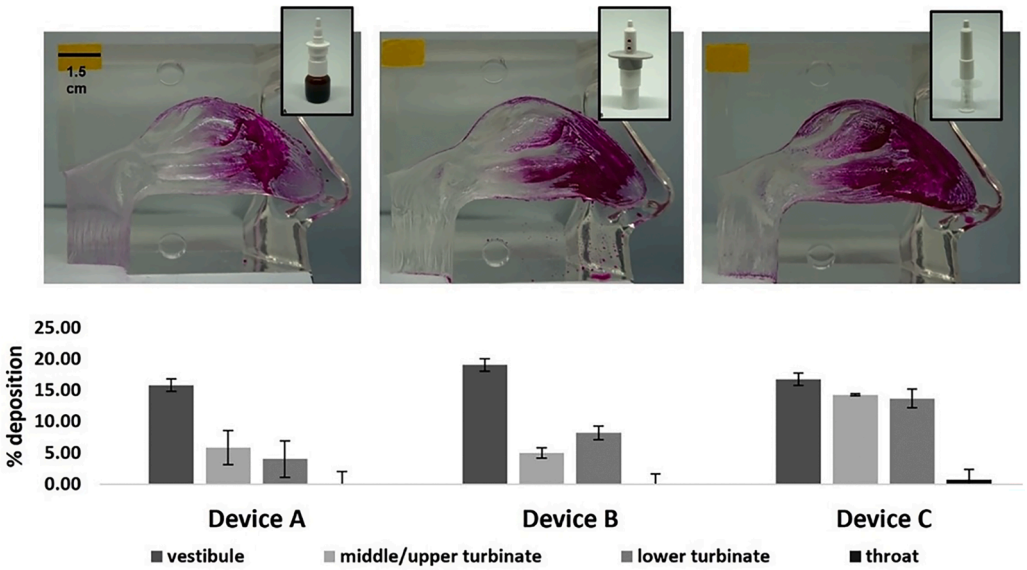

Fig. 7. the different distribution profile of the HL micelles obtained by administering the micellar formulation into a simulated nasal cavity using the three different nasal devices tested. Above, a visual representation of the nasal areas reached by the formulation once sprayed into the nostril. Below, a graphical representation of the distribution of the micellar formulation into the different regions of the nasal cavity that are vestibulum, middle/upper turbinate, lower turbinate and throat.

results regardless the variability that naturally characterizes the biological tissues.

The poor tendency of the micelles to stick to the mucus layer could also be attributed to the PEGylated hydrophilic surface of micelles provided by TPGS. In fact, PEG surface modification has been demonstrated to be able to reduce protein surface adhesion in a number of nanomaterials (Lai et al., 2007; Suk et al., 2016; Tang et al., 2009; Wang et al., 2008; Xu et al., 2015), as well as to avoid interactions with mucin glycoproteins in the mucus layer (Lai et al., 2007).

These structural features suggest a mucopenetration ability of the formulation, that could provide an escape strategy from the physiological process of muco-ciliary clearance, thus increasing the retention time in the nasal cavity. For this reason, the propensity of the developed micelles to penetrate mucus was tested and confirmed by diffusion results obtained by SAXS and successively by *ex vivo* mucoadhesion studies on rabbit nasal mucosa. Results indicate that micelles are able to enter and permeate together with water into a viscous mucin solution (15% w/v), used as mucus model, with a diffusion speed of the order of 10 μm/s, comparable with the one observed using a simulated nasal fluid alone. This was further explained by the fact that the very small particle size (about 12 nm) and the almost spherical shape can ensure that the micelles are not retained by the size filter consisting of the mucin fiber mesh, which porosity has been indicated between 50 and 1800 nm (Bansil et al., 1995; Lai et al., 2009).

The suitability of the micellar formulation for intranasal application was further confirmed by the administration of the micellar formulation in a nasal cast using different devices. The good distribution profile obtained and the absence of dripping regardless of the kind of device confirmed that the developed micelles could actually be exploited as an intranasal treatment. In particular, giving the more homogeneous distribution between the regions of the nose and the greater covered surface area obtained using the BiVax nasal atomizer (device **C**) as well as the best stability results obtained in terms of micelles size and PDI after administration, we believe that this is the most suitable device to guarantee greater protection against SARS-CoV-2 infection in the upper airways. Indeed, it should be considered that the nasal cavity represents a very large surface to which the virus can adhere after being inhaled giving rise to a starting infection. Considering that the greater the covered nasal surface, the higher the protective activity of the micellar formulation, the BiVax nasal atomizer was preferred to the other two tested nasal devices, because it has been shown to be able to distribute the micellar formulation more deeply in the nasal cavity leading to the greatest surface coverage, justified by the spray characterization results which showed a larger plume diameter and area for this nasal device which led to the greater and more homogenous cover of the nasal cavity.

Concerning the antiviral effect of the formulations tested, all the drug-loaded micelles showed significantly higher antiviral efficacy than pure CSA and the blank formulations. The only exception was represented by the LL micelles used to pre-treat infected cells. In this specific case indeed, the activity of the blank and the drug-loaded micelles did not differ, probably due to the very low concentration of CSA.

By comparing the results obtained with different treatment protocols, it was found that the best approaches to hinder the viral replication consist in a post-treatment 2 hours after infection or protocols in which repeated treatments are combined pre- or post-infection, simulating a repeated administration, a quite common and realistic situation for nasal medicinal products.

Concerning the three different formulations tested, the results obtained by testing the HL and ML micelles could be commented parallelly, since showed a similar behavior which was slightly different from that obtained by testing the LL micelles. In fact, when the ML and HL micelles were tested at the lowest CSA concentration (2 μM), the inhibition of the SARS-CoV-2 replication turned out to be the most effective, resulting greater than 100% in all the cases. On the contrary, the same results in terms of antiviral efficiency were obtained when the LL micelles were used at the highest CSA concentration, *i.e.* 8 μM. This difference could be attributed to a potential role of TPGS which, at each CSA concentration tested, was proportionally more abundant in the LL micelles, due to the lower drug content. This hypothesis is supported by the fact that by testing the blank micelles we observed a noticeable antiviral activity, even if significatively lower than that of the loaded micelles. In particular, a linear correlation between the blank micellar concentration used and the Cycle Threshold (Ct) value was found, indicating a reduction in the viral activity and replication. Firstly, given the surfactant properties of the polymer, we can attribute the antiviral activity of the blank micelles to the ability of TPGS to alter the fluidity of the viral envelop, by interpolation between phospholipids (Ostacolo et al., 2013; Shahab et al., 2022). Another possible mechanism has been reported by researchers from the University of Alabama at Birmingham (Birmingham, AL, USA). Their data, published as pre-print (Pacl et al., 2021)

demonstrated the capacity of water-soluble tocopherol derivatives, (specifically TPGS and, albeit to a lesser extent, also Vitamin E succinate) to inhibit the transcriptional activity of SARS-CoV-2 RNA-dependent RNA polymerase.

However, despite the blank micelles had also shown this kind of activity, we exclude that the effect belonged only to the presence of TPGS, but hypothesized a synergistic action of TPGS with CSA, since the percentages of infectivity reduction were significatively higher for almost all the drug-loaded micelles tested than for the blank micelles.

Indeed, when the non-formulated CSA was used as control, its effectiveness was dramatically lower than that shown when loaded into the micellar structure. In most cases, pure CSA antiviral activity did not exceed 50% which however was registered only working at the highest drug concentration, *i.e.* 32 μM. An exception occurred when pure CSA was present with the virus at the moment of the infection, where an inhibition up to 100% was attained. This is consistent with data reported in literature (de Wilde et al., 2011; Liu et al., 2020), attesting that CSA mainly acts on the very first phases of infection by altering the organization of the viral intracellular membranes exploited to generate the viral replication complex, which normally forms early after the cell penetration. However, this action seemed to prevail on another CSA antiviral action reported in literature, which consists in the hindering of the N protein's folding and its subsequent binding with the viral genome to assemble the viral progeny (Ma-Lauer et al., 2020).

On the contrary, CSA encapsulated in a micellar formulation based on TPGS underwent a significative improvement of its antiviral activity even at the lowest concentration tested, 2 μM. This is due to the presence of TPGS, that can have a series of actions enabling a more effective antiviral activity: 1) improvement of CSA solubility, making the peptide more available at molecular level; 2) enhanced CSA cell penetration, an effect related to the surface active properties of TPGS; 3) potential hindering of the receptor-ligand interactions normally exploited by the virus to infect cells (Angelini et al., 2013; Lundin et al., 2014; Oudshoorn et al., 2017), allowing the CSA micellar formulation to be effective at inhibiting SARS-CoV-2 infection even when used as a pre-treatment. Furthermore, we can also hypothesize that the well-known activity of TPGS as P-glycoprotein (P-gp) efflux inhibitor (Collnot et al., 2010) could contribute to the result, since it has been demonstrated in CaCo-2 (Augustijns et al., 1993), that CSA transport is modulated by these systems. Finally, the antioxidant activity of TPGS could be exploited in the most severe cases of infection, since it undergoes degradation leading to the release of vitamin E (Grimaudo et al., 2018) which can help to avoid the worsening of the disease. It is known indeed, that the viral infection causes an alteration of the balance between the production of oxidants and antioxidants leading to an oxidative stress responsible for serious complications (Laforge et al., 2020).

When the ML micelles and HL micelles were applied on cells 6 hours after infection, the antiviral activity was lower than the cases in which were applied following the other approaches. Our hypothesis was that after 6 hours from the infection, the replicative cycle of the virus is in an advanced phase, with the virus completely penetrated the cell starting its replication. At that point, as also reported in literature (de Wilde et al., 2011), neither the peptide drug, nor the TPGS could interfere with the viral replication leading to a completely inhibition of the infection. However, it must be underlined that despite the reduced antiviral activity demonstrated in this case by all the drug-loaded micelles, the effectiveness of the latter always demonstrated to be greater than that of the blank micelles and in most cases also of the non-formulated CSA, with the only exception represented by the cases in which the loaded micelles were diluted so as to work at concentrations of CSA of 2 μM: in these cases the level of efficacy of the drug loaded micelles was comparable to that of the blank micelles.

By making a general overview of the collected data, it can be appreciated that in several cases the viral inhibition corresponded to or exceeded the 100% value, indicating that viral replication was completely blocked. Values exceeding 100% were due to the fact that, after the replication of the virions had been blocked by the treatment, the virions remained in solution and started to degrade. The extent to which the virus degrades and therefore how much the percentage could be higher than 100 is a totally random factor. However, we noted a direct proportion between the concentration of the micelles and the percentage of viral inhibition, leading to confirm the hypothesis that the micelles were able to degrade the virus in solution.

Concerning the spray characteristics and deposition in the nasal cavity, anyone of the three devices tested did affect the physical properties of the micelles, preserving their size and surface charge. Sprays did not appear to differ in a significant manner in terms of emitted droplet size distribution, spray angle and spray plume characteristics. However, the device BiVax provided a significantly better coverage of the nasal cast both in terms of overall surface area covered and distribution over different region of interest such as upper and lower turbinates. This was attribute to a higher surface spray area that was correlated with the larger emitted volume (250 μL against 100 and 70 μL for BiDose and CPS device, respectively). This result is in agreement with the observations of Kundoor and Dalby (Kundoor and Dalby, 2011), that using the same cast, found that spray pumps delivering 100 μL had significantly greater nasal deposition area than nasal spray pumps delivering 50 μL. However, the deposition observed were mainly in the vestibule part of the nasal cavity, demonstrating that the choice of an optimal combination between device and formulation is required in order to develop a nasal product truly effective against a viral infection. In fact, the penetration of the formulation and coverage of nasal anatomical structures such as the turbinates involved in the filtration and entrapment of the particulate carried by inhaled air appears critical to prevent or treat early SARS-CoV-2 infections.

5. Conclusion

All the CSA-loaded micellar formulation developed in the present work showed high industrial scalability due to their simple and fast production method, and to the possibility of an easy sterilization by filtration. At the same time, the formulation resulted stable for at least 7 months at ambient temperature. Moreover, the low particle size, the almost neutral surface and the high rate of mucopenetration make them ideal for intranasal administration. The high drug encapsulation efficiency of the TPGS micelles was also exploited in our research to increase the low solubility of cyclosporine A, an immunosuppressant drug tested in this work for its potential as antiviral agent. The results obtained in an *in vitro* model of infection of SARS-CoV-2 Omicron variant highlighted that the drug-loaded micelles provided an excellent viral replication inhibition for single and repeated treatments pre-infection and up to 6 hours post-infection. In addition, CSA-loaded micelles performed better than CSA alone or the blank formulation at inhibiting the SARS-CoV-2 replication. Particularly, it was evidenced that also the micelle-forming excipient, the vitamin E derivative TPGS, plays a critical role in enhancing CSA inhibition of the viral replication, probably itself having an antiviral action through nonspecific mechanisms. Finally, the *in vivo* administration of the highest drug-loaded micellar formulation was simulated using a silicone human nasal cast after the *in vitro* characterization of the spray emitted by different systems, which allowed to identify a device able to deposit the micellar formulation homogeneously within the nasal cavity once intranasally administered, potentially providing a more effective protection against an incipient infection.

Author contribution

Conception and design, FG, FS; analysis and interpretation of the data, FG, FS, EDF, CR, LC, MB, IR; drafting of the paper, FG, FS, EDF, CR, IR; revising it critically for intellectual content, FS, SP, SN, EDF, CR; final approval of the version to be published, DD, FB, RB. All authors agree to

be accountable for all aspects of the work.

Supporting Information

The Supporting Information is available free of charge.

Isothermal stability of micelles at 25°C over 7 months; dynamic viscosity calculated at both 25°C and 37°C; Fitting parameters for SANS data; *in vitro* antiviral activity against 0.0005 m.o.i; *p* values obtained by the statistical analysis.

Declaration of Competing Interest

The authors declare no conflict of interest.

Data availability

The data supporting this work are accessible upon reasonable request from the corresponding author.

Aknowledgements

E.D.F. acknowledges the UniMi support (PSR2021_DEL_FAVERO). The authors are grateful for beam-time allocation and financial support to ESRF (DOI: 10.15151/ESRF-ES-653835676) and to CERIC (CERIC_20217127). This work benefited from the use of the SasView application for SANS and SAXS analysis.

Supplementary materials

Supplementary material associated with this article can be found, in the online version, at doi:10.1016/j.ejps.2023.106673.

References

Ammerman, N., Beier-Sexton, M., Azad, A., 2008. Growth and maintenance of Vero cell lines. CurrProtoc Microbiol 4, 4.

Angelini, M.M., Akhlaghpour, M., Neuman, B.W., Buchmeier, M.J., 2013. Severe Acute Respiratory Syndrome Coronavirus Nonstructural Proteins 3, 4, and 6 Induce Double-Membrane Vesicles. MBio 4 (4), 00524-13.

Augustijns, P.F., Bradshaw, T.P., Gan, L.S.L., Hendren, R.W., Thakker, D.R., 1993. Evidence for a Polarized Efflux System in Caco-2 Cells Capable of Modulating Cyclosporine A Transport. *Biochem. Biophys. Res. Commun* 197 (2), 360–365.

Bansil, R., Stanley, E., Lamont, J.T., 1995. Mucin Biophysics. Annu. Rev. Physiol. 57 (1), 635–657.

Berton, P., Mishra, M.K., Choudhary, H., Myerson, A.S., Rogers, R.D., 2019. Solubility Studies of Cyclosporine Using Ionic Liquids. ACS Omega 4 (5), 7938–7943.

Bleier, B.S., Ramanathan, M., Lane, A.P., 2020. COVID-19 Vaccines May Not Prevent Nasal SARS-CoV-2 Infection and Asymptomatic Transmission. Otolaryngol. Neck Surg. 164 (2), 305–307.

Burnett, L., McQueen, M., Jonsson, J., Torricelli, F., 2007. IFCC Position Paper: Report of the IFCC Taskforce on Ethics: Introduction and framework. Clin Chem Lab Med 45, 1098–1104.

Castile, J., Cheng, Y.H., Simmons, B., Perelman, M., Smith, A., Watts, P., 2013. Development of in vitro models to demonstrate the ability of PecSys®, an in situ nasal gelling technology, to reduce nasal run-off and drip. Drug Dev. Ind. Pharm. 39 (5), 816–824.

Chavda, V.P., Baviskar, K.P., Vaghela, D.A., Raut, S.S., Bedse, A.P., 2023. Nasal sprays for treating COVID-19: a scientific note. *Pharmacol. Reports* 75, 249–265.

Chavda, V.P., Vora, L.K., Pandya, A.K., Patravale, V.B., 2021. Intranasal vaccines for SARS-CoV-2: From challenges to potential in COVID-19 management. *Drug Discov. Today* 26, 2619–2636.

Chen, N., Zhou, M., Dong, X., Qu, J., Gong, F., Han, Y., Qiu, Y., Wang, J., Liu, Y., Wei, Y., Xia, J., Yu, T., Zhang, X., Zhang, L., 2020. Epidemiological and clinical characteristics of 99 cases of 2019 novel coronavirus pneumonia in Wuhan, China: a descriptive study. Lancet 395 (10223), 507–513.

Clementino, A.R., Pellegrini, G., Banella, S., Colombo, G., Cantù, L., Sonvico, F., Del Favero, E., 2021. Structure and Fate of Nanoparticles Designed for the Nasal Delivery of Poorly Soluble Drugs. Mol. Pharm. 18 (8), 3132–3146.

Collnot, E.M., Baldes, C., Schaefer, U.F., Edgar, K.J., Wempe, M.F., Lehr, C.M., 2010. Vitamin TPGS P-Glycoprotein Inhibition Mechanism: Influence on Conformational Flexibility, Intracellular ATP Levels, and Role of Time and Site of Access. Mol. Pharm 7 (3), 642–651.

De Wilde, A.H., Zevenhoven-Dobbe, J.C., van der Meer, Y., Thiel, V., Narayanan, K., Makino, S., Snijder, E.J., van Hemert, M.J., 2011. Cyclosporin A inhibits the replication of diverse coronaviruses. J. Gen. Virol. 92 (11), 2542–2548.

Di Cola, E., Cantù, L., Brocca, P., Rondelli, V., Fadda, G.C., Canelli, E., Martelli, P., Clementino, A.R., Sonvico, F., Bettini, R., Del Favero, E., 2019. Novel O/W nanoemulsions for nasal administration: Structural hints in the selection of performing vehicles with enhanced mucopenetration. Colloids Surfaces B Biointerfaces 183, 110439.

Eichner, H., Behbehani, A.A., Hochstrasser, K., 1983. Diagnostic value of nasal secretions, current state: normal values. Laryngol. Rhinol. Otol. 62 (12), 561–565.

El Tayar, N., Mark, A.E., Vallat, P., Brunne, R.M., Testa, B., van Gunsteren, W.F., 1993. Solvent-Dependent Conformation and Hydrogen-Bonding Capacity of Cyclosporin A: Evidence from Partition Coefficients and Molecular Dynamics Simulations. J. Med. Chem. 36 (24), 3757–3764.

Ghezzi, M., Ferraboschi, I., Delledonne, A., Pescina, S., Padula, C., Santi, P., Sissa, C., Terenziani, F., Nicoli, S., 2022. Cyclosporine-loaded micelles for ocular delivery: Investigating the penetration mechanisms. J. Cont. Release 349, 744–755.

Ghezzi, M., Pescina, S., Padula, C., Santi, P., Del Favero, E., Cantù, L., Nicoli, S., 2021. Polymeric micelles in drug delivery: An insight of the techniques for their characterization and assessment in biorelevant conditions. J. Control. Release. 332, 312–336.

Gorbalenya, A.E., Baker, S.C., Baric, R.S., de Groot, R.J., Drosten, C., Gulyaeva, A.A., Haagmans, B.L., Lauber, C., Leontovich, A.M., Neuman, B.W., Penzar, D., Perlman, S., Poon, L.L.M., Samborskiy, D.V., Sidorov, I.A., Sola, I., Ziebuhr, J., 2020. Coronaviridae Study Grp, The species Severe acute respiratory syndrome-related coronavirus: classifying 2019-nCoV and naming it SARS-CoV-2. Nat. Microbiol. 5 (4), 536–544.

Grimaudo, M.A., Nicoli, S., Santi, P., Concheiro, A., Alvarez-Lorenzo, C., 2018. Cyclosporine-loaded cross-linked inserts of sodium hyaluronan and hydroxypropyl-β-cyclodextrin for ocular administration. Carbohydr. Polym. 201, 308–316.

Grimaudo, M.A., Pescina, S., Padula, C., Santi, P., Concheiro, A., Alvarez-Lorenzo, C., Nicoli, S., 2018. Poloxamer 407/TPGS Mixed Micelles as Promising Carriers for Cyclosporine Ocular Delivery. Mol. Pharm. 15 (2), 571–584.

Guo, J., Wu, T., Ping, Q., Chen, Y., Shen, J., Jiang, G., 2005. Solubilization and Pharmacokinetic Behaviors of Sodium Cholate/Lecithin-Mixed Micelles Containing Cyclosporine A. *Drug Deliv*. J. Deliv. Target. Ther. Agents. 12 (1), 35–39.

Hu, B., Guo, H., Zhou, P., Shi, Z.L., 2021. Characteristics of SARS- CoV-2 and COVID-19. Nat. Rev. Microbiol. 19 (3), 141–154.

Kundoor, V., Dalby, R.N., 2011. Effect of formulation- and administration-related variables on deposition pattern of nasal spray pumps evaluated using a nasal cast. Pharm. Res. 28 (8), 1895–1904.

Laforge, M., Elbim, C., Frère, C., Hémadi, M., Massaad, C., Nuss, P., Benoliel, J., Becker, C., 2020. Tissue damage from neutrophil-induced oxidative stress in COVID-19 Mireille. Nat. Rev. Immunol. 20 (9), 515–516.

Lai, S.K., O'Hanlon, D.E., Harrold, S., Man, S.T., Wang, Y., Cone, R., Hanes, J., 2007. Rapid transport of large polymeric nanoparticles in fresh undiluted human mucus. Proc. Natl. Acad. Sci 104 (5), 1482–1487.

Lai, S.K., Wang, Y.Y., Wirtz, D., Hanes, J., 2009. Micro- and macrorheology of mucus. Adv. Drug Deliv. Rev. 61 (2), 86–100.

Lallemand, F., Felt-Baeyens, O., Besseghir, K., Behar-Cohen, F., Gurny, R., 2003. Cyclosporine A delivery to the eye: A pharmaceutical challenge. Eur. J. Pharm. Biopharm. 56 (3), 307–318.

Lallemand, F., Perottet, P., Felt-Baeyens, O., Kloeti, W., Philippoz, F., Marfurt, J., Besseghir, K., Gurny, R., 2005. A water-soluble prodrug of cyclosporine A for ocular application: A stability study. Eur. J. Pharm. Sci. 26 (1), 124–129.

Lallemand, F., Schmitt, M., Bourges, J.L., Gurny, R., Benita, S., Garrigue, J.S., 2017. Cyclosporine A delivery to the eye: A comprehensive review of academic and industrial efforts. Eur. J. Pharm. Biopharm. 117, 14–28.

Larhed, A.W., Artursson, P., Gråsjö, J., Björk, E., 1997. Diffusion of Drugs in Native and Purified Gastrointestinal Mucus. J. Pharm. Sci. 86 (6), 660–665.

Lei, C., Yang, J., Hu, J., Sun, X., 2020. On the Calculation of TCID50 for Quantitation of Virus Infectivity. Virol. Sin. 12250.

Liu, C., von Brunn, A., Zhu, D., 2020. Cyclophilin A and CD147: novel therapeutic targets for the treatment of COVID-19. Med. Drug Discov. 7, 100056.

Luschmann, C., Tessmar, J., Schoeberl, S., Strau, O., Luschmann, K., Goepferich, A., 2014. Self-Assembling Colloidal System for the Ocular Administration of Cyclosporine A. Cornea 33, 1.

Lundin, A., Dijkman, R., Bergström, T., Kann, N., Adamiak, B., Hannoun, C., Kindler, E., Jónsdóttir, H.R., Muth, D., Kint, J., Forlenza, M., Müller, M.A., Drosten, C., Thiel, V., Trybala, E., 2014. Targeting Membrane-Bound Viral RNA Synthesis Reveals Potent Inhibition of Diverse Coronaviruses Including the Middle East Respiratory Syndrome Virus. PLOS Pathog 10 (5), 1–15.

Mahajan, H.S., Gattani, S.G., 2009. Gellan gum based microparticles of metoclopromide hydrochloride for intranasal delivery: Development and evaluation. Chem. Pharm. Bull. 57 (4), 388–392.

Ma-Lauer, Y., Zheng, Y., Malešević, M., von Brunn, B., Fischer, G., von Brunn, A., 2020. Influences of cyclosporin A and non-immunosuppressive derivatives on cellular cyclophilins and viral nucleocapsid protein during human coronavirus 229E replication. Antiviral Res 173, 104620.

Mamatis, J.E., Pellizzari-Delano, I.E., Gallardo-Flores, C.E., Colpitts, C.C., 2022. Emerging Roles of Cyclophilin A in Regulating Viral Cloaking. Front. Microbiol. 13, 1–8.

Mehta, P., McAuley, D.F., Brown, M., Sanchez, E., Tattersall, R.S., Manson, J.J., 2020. COVID-19: consider cytokine storm syndromes and immunosuppression. Lancet 395 (10229), 1033–1034.

Munda, R., Schroeder, T.J., Pedersen, S.A., Clardy, C.W., Wadhwa, N.K., Myre, S.A., Stephens, S.A., Pesce, G.W., Alexander, A.J., 1988. Cyclosporine pharmacokinetics in pancreas transplant Recipients. Transplant. Proc 20 (2), 487—490.

Ostacolo, C., Caruso, C., Tronino, D., Troisi, S., Laneri, S., Pacente, L., Del Prete, A., Sacchi, A., 2013. Enhancement of corneal permeation of riboflavin-5′-phosphate through vitamin E TPGS: A promising approach in corneal trans-epithelial cross linking treatment. Int. J. Pharm. 440 (2), 148–153.

Oudshoorn, D., Rijs, K., Limpens, R.W.A.L., Groen, K., Koster, A.J., Snijder, E.J., Kikkert, M., Bárcena, M., 2017. Expression and Cleavage of Middle East Respiratory Syndrome Coronavirus nsp3-4 Polyprotein Induce the Formation of Double-Membrane Vesicles That Mimic Those Associated with Coronaviral RNA Replication. MBio 8 (6), 1658-17.

UAB Precision Medicine Institute Pacl, H.T.Pacl, Tipper, J.L., Sevalkar, R.R., Crouse, A., Crowder, C., Ahmad, S., Ahmad, A., Holder, G.D., Kuhlman, C.J., Chinta, K.C., Nadeem, S., Green, T.J., Petit, C.M., Steyn, A.J.C., Mightet, M., 2021. Water-soluble tocopherol derivatives inhibit SARS-CoV-2 RNA-dependent RNA polymerase, (Preprint). bioRxiv, 2021.07.13.449251, submitted: Jul 2021.

Patel, A., Cholkar, K., Agrahari, V., Mitra, A.K., 2013. Ocular drug delivery systems: An overview. World J. Pharmacol. 2 (2), 47–64.

Peel, M., Scribner, A., 2013. Cyclophilin inhibitors as antiviral agents. Bioorganic Med. Chem. Lett. 23 (16), 4485–4492.

Pepić, I., Lovrić, J., Filipović-Grčić, J., 2013. How do polymeric micelles cross epithelial barriers? Eur. J. Pharm. Sci. 50 (1), 42–55.

Pescina, S., Grolli Lucca, L., Govoni, P., Padula, C., Del Favero, E., Cantù, L., Santi, P., Nicoli, S., 2019. Ex Vivo Conjunctival Retention and Transconjunctival Transport of Poorly Soluble Drugs Using Polymeric Micelles. Pharmaceutics 11, 9.

Pescina, S., Sonvico, F., Clementino, A., Padula, C., Santi, P., Nicoli, S., 2021. Preliminary Investigation on Simvastatin-Loaded Polymeric Micelles in View of the Treatment of the Back of the Eye. Pharmaceutics 13, 6.

Pfefferle, S., Schöpf, J., Kögl, M., Friedel, C.C., Müller, M.A., Carbajo-Lozoya, J., Stellberger, T., von Dall'Armi, E., Herzog, P., Kallies, S., Niemeyer, D., Ditt, V., Kuri, T., Züst, R., Pumpor, K., Hilgenfeld, R., Schwarz, F., Zimmer, R., Steffen, I., Weber, F., Thiel, V., Herrler, G., Thiel, H., Schwegmann-Weßels, C., Pöhlmann, S., Haas, J., Drosten, C., von Brunnet, A., 2011. The SARS-Coronavirus-Host Interactome: Identification of Cyclophilins as Target for Pan-Coronavirus Inhibitors. PLoS Pathog 7, 10.

Puig-Rigall, J., Grillo, I., Dreiss, C.A., González-Gaitano, G., 2017. Structural and Spectroscopic Characterization of TPGS Micelles: Disruptive Role of Cyclodextrins and Kinetic Pathways. Langmuir 33 (19), 4737–4747.

Reed, L., Muench, H., 1938. A simple method of estimating fifty per cent endpoints. Am. J. Epidemiol. 27 (3), 493–497.

Schreiber, S.L., Crabtree, G.R., 1992. The mechanism of action of cyclosporin A and FK506. Immunol. Today. 13 (4), 136–142.

Shahab, M.S., Rizwanullah, M., Sarim Imam, S., 2022. Formulation, optimization and evaluation of vitamin E TPGS emulsified dorzolamide solid lipid nanoparticles. J. Drug Deliv. Sci. Technol. 68, 103062.

Sonvico, F., Colombo, G., Quarta, E., Guareschi, F., Banella, S., Buttini, F., Scherließ, R., 2023. Nasal delivery as a strategy for the prevention and treatment of COVID-19. Expert Opin. Drug Deliv. 20, 1115–1130.

Stadnytskyi, V., Bax, C.E., Bax, A., Anfinrud, P., 2020. The airborne lifetime of small speech droplets and their potential importance in SARS-CoV-2 transmission. Proc. Natl. Acad. Sci. U. S. A. 117 (22), 11875–11877.

Stetefeld, J., McKenna, S.A., Patel, T.R., 2016. Cyclosporine A delivery to the eye: Dynamic light scattering: a practical guide and applications in biomedical sciences. Biophys. Rev. 8 (4), 409–427.

Suk, J.S, Xu, Q., Kim, N., Hanes, J., Ensign, L.M., 2016. PEGylation as a strategy for improving nanoparticle-based drug and gene delivery. Adv. Drug Deliv. Rev. 99, 28–51.

Sweeney, Z.K., Fu, J., Wiedmann, B., 2014. From Chemical Tools to Clinical Medicines: Nonimmunosuppressive Cyclophilin Inhibitors Derived from the Cyclosporin and Sanglifehrin Scaffold. J. Med. Chem. 57 (17), 7145–7159.

Tandon, M., Wu, W., Moore, K., Winchester, S., Tu, Y.-P., Miller, C., Kodgule, R., Pendse, A., Rangwala, S., Joshi, S., 2022. SARS-CoV-2 accelerated clearance using a novel nitric oxide nasal spray (NONS) treatment: A randomized trial. *Lancet Reg. Heal.* - Southeast Asia 3, 100036.

Tang, B.C., Dawson, M., Lai, S.K., Hanes, J., 2009. Biodegradable polymer nanoparticles that rapidly penetrate the human mucus barrier. Proc. Natl. Acad. Sci. U. S. A. 106 (46), 19268–19273.

Wang, Y.Y., Lai, S.K., Suk, J.S., Pace, A., Cone, R., Hanes, J., 2008. Addressing the PEG Mucoadhesivity Paradox to Engineer Nanoparticles that "Slip" through the Human Mucus Barrier. Angew. Chemie. 120 (50), 9872–9875.

Wölfel, R., Corman, V.M., Guggemos, W., Seilmaier, M., Zange, S., Müller, M.A., Niemeyer, D., Jones, T.C., Vollmar, P., Rothe, C., Hoelscher, M., Bleicker, T., Brünink, S., Schneider, J., Ehmann, R., Zwirglmaier, K., Drosten, C., WendtnerRet, C., 2020. Virological assessment of hospitalized patients with COVID-2019. Nature 581 (7809), 465–469.

Wu, J.T., Leung, K., Leung, G.M., 2020. Nowcasting and forecasting the potential domestic and international spread of the 2019-nCoV outbreak originating in Wuhan, China: a modelling study. Obstet. Gynecol. Surv. 75 (7), 399–400.

Xu, Q., Ensign, L.M., Boylan, N.J., Schön, A., Gong, X., Yang, J., Lamb, N.W., Cai, S., Yu, T., Freire, E., Hanes, J., 2015. Impact of Surface Polyethylene Glycol (PEG) Density on Biodegradable Nanoparticle Transport in Mucus ex Vivo and Distribution in Vivo. ACS Nano 9 (9), 9217–9227.

Yu, Y., Chen, D., Li, Y., Yang, W., Tu, J., Shen, Y., 2018. Improving the topical ocular pharmacokinetics of lyophilized cyclosporine A-loaded micelles: formulation, in vitro and in vivo studies. Drug Deliv 25 (1), 888–899.

Zou, L., Ruan, F., Huang, M., Liang, L., Huang, H., Hong, Z., Yu, J., Song, Y., Xia, J., Guo, Q., Song, T., He, J., Yen, H., Peiris, M., Wu, J., 2020. SARS-CoV-2 Viral Load in Upper Respiratory Specimens of Infected Patients. N. Engl. J. Med. 382 (12), 1177–1179.